Biochimica et Biophysica Acta 1828 (2013) 801–815

Contents lists available at SciVerse ScienceDirect

Biochimica et Biophysica Acta

journal homepage: www.elsevier.com/locate/bbamem

Effects of surfactin on membrane models displaying lipid phase separation

Magali Deleu [a,*,1], Joseph Lorent [b,1], Laurence Lins [c], Robert Brasseur [c], Nathalie Braun [d], Karim El Kirat [d], Tommy Nylander [e], Yves F. Dufrêne [d], Marie- Paule Mingeot-Leclercq [b]

[a] Université de Liège, Gembloux Agro-Bio Tech, Unité de Chimie Biologique Industrielle, Passage des Déportés, 2, B-5030 Gembloux, Belgium
[b] Université Catholique de Louvain, Louvain Drug Research Institute, Cellular and Molecular Pharmacology, Avenue E. Mounier 73, B1.73.05, B-1200, Brussels, Belgium
[c] Université de Liège, Gembloux Agro-Bio Tech, Centre de Biophysique Moléculaire Numérique, Passage des Déportés, 2, B-5030 Gembloux, Belgium
[d] Université Catholique de Louvain, Institute of Condensed Matter and Nanosciences, Bio and Soft Matter, Croix du Sud 1, L7.04.01, B-1348 Louvain-la-Neuve, Belgium
[e] Lund University, Center for Chemistry and Chemical Engineering, Physical Chemistry, 1S-221 00 Lund, Sweden

ARTICLE INFO

Article history:
Received 20 July 2012
Received in revised form 19 October 2012
Accepted 5 November 2012
Available online 14 November 2012

Keywords:
Surfactin
Membrane interaction
Phase coexistence
Laurdan and DPH fluorescence
Ellipsometry
AFM

ABSTRACT

Surfactin, a bacterial amphiphilic lipopeptide is attracting more and more attention in view of its bioactive properties which are in relation with its ability to interact with lipids of biological membranes. In this work, we investigated the effect of surfactin on membrane structure using model of membranes, vesicles as well as supported bilayers, presenting coexistence of fluid-disordered (DOPC) and gel (DPPC) phases. A range of complementary methods was used including AFM, ellipsometry, dynamic light scattering, fluorescence measurements of Laurdan, DPH, calcein release, and octadecylrhodamine B dequenching. Our findings demonstrated that surfactin concentration is critical for its effect on the membrane. The results suggest that the presence of rigid domains can play an essential role in the first step of surfactin insertion and that surfactin interacts both with the membrane polar heads and the acyl chain region. A mechanism for the surfactin lipid membrane interaction, consisting of three sequential structural and morphological changes, is proposed. At concentrations below the CMC, surfactin inserted at the boundary between gel and fluid lipid domains, inhibited phase separation and stiffened the bilayer without global morphological change of liposomes. At concentrations close to CMC, surfactin solubilized the fluid phospholipid phase and increased order in the remainder of the lipid bilayer. At higher surfactin concentrations, both the fluid and the rigid bilayer structures were dissolved into mixed micelles and other structures presenting a wide size distribution.

1. Introduction

Surfactin, a bacterial lipopeptide [1,2] has a structure consisting of a cyclic heptapeptide headgroup with the sequence Glu-Leu-D-Leu-Val-Asp-D-Leu-Leu linked to a $C_{13–15}$ β-hydroxy fatty acid by a lactone bond. The β-hydroxy fatty acid chain of the homologues C13 and C15 are branched (isopropyl group at the chain end) while the one of the homologue C14 is linear. The two negatively-charged amino acids, which form a polar head opposite to the five lipophilic amino acids, and the hydrocarbon side chain account for the amphiphilic nature of surfactin and its strong surfactant properties [3,4]. Surfactin is attracting more and more attention in view of its many interesting bioactive properties. These include the lipopeptides potential as antiviral [5,6], antimycoplasma [7] and antibacterial agent [8–10] as well as its capacity as anti-adhesive agent against pathogenic bacteria [11], insecticide [12], antihypercholesterolemia agent [13], inflammation suppressor [14] and plant defense elicitor [15]. However it has also been reported to have hemolytic [16] and apoptotic [17] properties. It is generally accepted that these properties are directly related to the interaction of surfactin with the lipid component of the biological membranes, which eventually leads to membrane destabilization [18–23]. Surfactin interaction with the membrane is highly dependent on the surfactin concentration [20,23–26]. Shen et al. [26] have suggested the need for a threshold concentration of surfactin in the bilayer for its solubilization. Several studies have shown that sensitivity of model membranes to surfactin is dependent on their lipid composition [24–31], and also on lipid organization (i.e. the physical state) [22]. Surfactin exhibits an enhanced binding to solid ordered domains-containing vesicles [22]. Carillo et al. [28] have also suggested that dipalmitoylphosphatidylcholine (DPPC), forming a gel phase in synthetic bilayers, acts as a promoter of surfactin-induced leakage. On the contrary, cholesterol and POPE attenuate the membrane-perturbing effect of surfactin. Most of these earlier studies have considered very simple biomimetic membrane systems with single phospholipid. Only both of them [22,28] have tackled the question of the effect of surfactin on mixtures of lipids which are more realistic models.

Regarding the role played by lipid domains for cell physiology, we investigated the effect of surfactin on the lateral heterogeneity of bilayers.

* Corresponding author. Tel.: +32 81 62 26 52; fax: +32 81 62 22 31.
E-mail address: magali.deleu@ulg.ac.be (M. Deleu).
[1] Co-first author.

0005-2736/$ – see front matter © 2012 Elsevier B.V. All rights reserved.
http://dx.doi.org/10.1016/j.bbamem.2012.11.007

Indeed, the more rigid lipid domains (ordered phase Lo) within cell membranes are suggested to participate as platforms [32] for many processes like signal transduction, disease pathogenesis and intracellular sorting [33,34].

The present study therefore aims to reveal the effect of surfactin on the lipid phase coexistence and especially on the coexistence of gel (DPPC) and disordered liquid (Ld) (dioleoylphosphatidylcholine DOPC) phases, which so far has not been addressed. For this purpose, we used Laurdan fluorescence technique and atomic force microscopy. Further information on the influence of surfactin insertion onto the transversal organization of the bilayer was obtained by DPH and Laurdan fluorescence measurements. As model for segregated bilayer system we used a 1:1 mol/mol DPPC:DOPC mixture, which is known to be segregated into microscopic domains of different fluidity [24,35]. Surfactin concentration known to have different effects on model membrane destabilization [20,23,25,36] is considered in this study. The interaction was quantified with ellipsometry and the experimental results, supported by molecular modeling, are used to reveal the modes of interaction and preferred location of surfactin at the microscopic and molecular level. Consequences of these microscopic and molecular effects on the macroscopic behavior of the lipid vesicles are investigated by size, fusion and permeability measurements. Implications of our results on the biological activity of surfactin are discussed.

2. Materials and methods

2.1. Materials

Dipalmitoylphosphatidylcholine (DPPC), dioleoylphosphatidylcholine (DOPC), β-D-dodecyl maltoside and calcein were purchased from Sigma (St. Louis, MO). The self-quenched fluorescent probe calcein was purified as described in detail previously [37]. Briefly, calcein was dissolved in 6 N NaOH and subjected to size-exclusion chromatography through a Sephadex® LH-20 column. The final concentration of the calcein solution in 20 mM Tris–HCl was 73 mM with an osmolality of 404 mOsm/kg (measured by the freezing point technique, using a Knauer osmometer automatic (Berlin, Germany). DPH (1,6-diphenyl-1,3,5-hexatriene), Laurdan (6-dodecanoyl-2-dimethyl-aminonaphtalene) and octadecylrhodamine B (R_{18}) were purchased from Molecular Probes (Invitrogen, Carlsbad, CA). Surfactin was produced by fermentation of *B. subtilis* S499 and isolated as described in detail previously [38]. The primary structure and purity of surfactin (>95%) were ascertained by analytical RP-HPLC (Vydack 10 μm C18 column, 0.46×25 cm, Vydack, Hesperia, CA), amino acid analysis, and MALDI-TOF mass spectrometry measurements (Ultraflex TOF, Bruckner, Karlsruhe, Germany). The surfactin mixture, 95.4% pure, was composed of surfactin-C13, -C14 and -C15 (0.3:1:1 mol/mol/mol). The homologues C13 and C15 comprise a branched β-hydroxy fatty acid chain (isopropyl group at the chain end) with 13 or 15 carbon atoms and the homologue C14 encloses a linear β-hydroxy fatty acid chain with 14 carbon atoms. All other products (grade 1) were purchased from Sigma-Aldrich (St-Louis, MO).

2.2. Preparation of liposomes

Liposomes were prepared from a mixture of DOPC:DPPC (1:1). For this purpose, the lipids were dissolved in chloroform:methanol (2:1, v:v) in a round bottomed flask. The solvent was evaporated under vacuum (Rotavapor R Buchi RE-111, Buchi, Flawil, Switzerland) to obtain a thin lipid film, which was dried overnight in a vacuum dessicator to remove remaining solvent. The dry lipid film was hydrated for 1 h with Tris 10 mM and NaCl 150 mM at pH 8.5 and 37 °C in a nitrogen atmosphere. This suspension was submitted to five cycles of freezing/thawing to obtain multilamellar vesicles (MLV). Depending on the type of experiment to be performed, this suspension was either sonicated to yield small unilamellar vesicles (SUV) [39] or extruded to produce large unilamellar vesicles (LUV) of 100 nm diameter [37]. The actual phospholipid content of each preparation was determined by phosphorus assay [40] and the concentration of liposomes was adjusted for each type of experiment.

2.3. Preparation of supported phospholipid bilayers (SPBs)

For surface analysis by atomic force microscopy, we prepared supported lipid bilayers using the vesicle fusion method [41]. DOPC and DPPC were dissolved in chloroform at 1 mM final concentration. An equimolar mixture of these two lipids was then evaporated under nitrogen and dried in a dessicator under vacuum for 2 h. Multilamellar vesicles (MLV) were obtained by resuspending the lipidic dried film in calcium-containing buffer (10 mM Tris, 150 mM NaCl and 3 mM $CaCl_2$ at pH 8.5) at 1 mM final lipid concentration. To obtain small unilamellar vesicles (SUV), the suspension was sonicated to clarity (4 cycles of 2 min) using a 500 W probe sonicator (Fisher Bioblock Scientific, France; 35% of the maximal power; 13 mm probe diameter) while keeping the suspension in an ice bath. The liposomal suspension was then filtered on 0.2 μm nylon filters (Whatman Inc., USA) to remove titanium particles coming from the sonicator tip. Freshly cleaved mica squares (16 mm^2) were glued onto steel sample pucks (Veeco Metrology LLC, Santa Barbara, CA) using Epotek 377 (Gentec Benelux, Waterloo, Belgium). Two milliliters of the SUV suspension were then deposited onto the mica samples and the SUVs were allowed to adsorb and fuse on the solid surface for 1 h at 60 °C. Subsequently, the sample was rinsed five times with Tris 10 mM and NaCl 150 mM at pH 8.5 to eliminate calcium and non-adsorbed vesicles. The samples were then slowly cooled to room temperature.

For ellipsometry investigations, supported lipid bilayers were formed *in situ* in the ellipsometer cuvette by co-adsorption of phospholipids (DOPC or DPPC) with β-D-dodecyl maltoside on hydrophilic silicon–silicon oxide surfaces as described by Vacklin [42]. A typical procedure for bilayer formation contains six stages: adsorption from a 6:1 (w/w%) mixture of β-D-dodecyl maltoside and the requisite phospholipid at a concentration of 0.114 g/l, followed by extensive dilution (rinsing) with 10 mM Tris and 150 mM NaCl at pH 7.4 buffer, and two readsorption steps from 10 and 100 times more dilute phospholipid/maltoside solutions respectively, each followed by rinsing.

2.4. Isothermal titration calorimetry

Critical micellar concentration (CMC) was determined using isothermal titration calorimetry (ITC) on a VP-ITC Microcalorimeter (Microcal, Northampton USA) at both pH 7.4 and 8.5 in 10 mM Tris and 150 mM NaCl buffer into milliQ water (Millipore Co., Milford, MA) at 25 °C. The CMC was determined by calorimetric dilution experiments [19]. The injection syringe was filled with a micellar solution of surfactin (0.3 mM or 0.08 mM). The sequential injection (6 μL) of the micellar solution into the 1.4565 mL calorimeter mixing cell containing only buffer, which was stirred at a speed of 305 rpm, lead to disintegration of the micelles into surfactin monomers until the concentration in the cell approaches the CMC. At this point, micelles were no longer dissociated. The disintegration process produced a heat of demicellization that is then measured by the calorimeter. The typical profile of the heat generated versus addition of the micellar surfactin stock solution was sigmoidal and the CMC was determined from the inflection point.

Prior to each analysis all solutions were degassed using a sonicator bath. The heats linked to buffer injection were determined by injecting buffer into buffer and substracted from the heats determined in the experiments. All measurements were repeated two times with two different surfactin solutions. Data were processed by using the software Origin 7 (Originlab, Northampton, USA).

2.5. Ellipsometry

Measurements of surface excess values and thickness of supported DPPC or DOPC bilayers in absence or in presence of increasing concentration of surfactin were performed by ellipsometry. Ellipsometry is based on monitoring of amplitude, ψ, and phase, Δ, changes of the compounds of polarized light upon reflection. The rate of data collection, with a time resolution of about 2 s, is fast enough for kinetic studies of lipid and surfactant adsorption. The instrument used was a Rudolph Research null-ellipsometer, model 43606-200E, equipped with a xenon arc lamp (Osram XBO 75 W/2) as a light source (λ = 250–1000 nm).

All measurements were performed with a light-source wavelength of 401.5 nm and with an angle of incidence of 68°. The 5 ml cuvette was thermostated at 25.0 °C ± 0.1 °C, and agitation of the solution in the cuvette was performed with a magnetic stirrer at about 300 rpm. The ellipsometric angles ψ and Δ were used to compute the complex reflection amplitude ratio ρ:

$$\rho = \left|r_p/r_s\right| \exp\left(\delta_{rp} - \delta_{rs}\right) = \tan\psi \exp(i\Delta) \quad (1)$$

where r_s and r_p are the reflection coefficients for s- and p-polarizations and δ_{rp} and δ_{rs} represent their phase shifts upon reflection.

In a typical ellipsometry experiment, the measurement was performed on silicon wafer (50 mm × 10 mm) slides pre-treated as described by Tiberg and Landgren [43] and pre-equilibrated overnight in a 10 mM Tris and 150 mM NaCl buffer at pH 7.4. Oxide layers were first characterized by four-zone measurements in air and in water after an equilibration period of 30 min, recording 6 minima in each zone as described in details by Landgren and Jönsson [44]. The substrate optical parameters were on average found to be n_2 (Si) = 5.50–0.25i and n_1 (SiO_2) = 1.49, and d_1 = 270–300 Å. After changing the cuvette content with 10 mM Tris and 150 mM NaCl buffer at pH 7.4 and an equilibration time of 30 min, supported lipid bilayers were formed as described above. The changes in ψ and Δ were monitored as a function of time at each stage of bilayer formation until only a very small change resulted from rinsing. At this point, surfactin stock solution in dimethylsulfoxide (DMSO) (1–10 mM) was added (1–40 μL) and the change in ellipsometric angles typically monitored over a period of 8–24 h. The volume of DMSO injected into the cuvette containing the buffer 10 mM Tris and 150 mM NaCl at pH 7.4 is below 1% of the total volume and has no influence on the measured parameters. The recorded ψ, and Δ values was evaluated assuming four-layer optical model where each layer is homogenous and assuming homogenous planar layers, using a numerical procedure originally devised by McCrackin et al. [45] as described by Tiberg and Landgren [43], and Landgren and Jönsson [44]. The obtained thickness, d, and refractive index, n, of the adsorbed layer can then be used to calculate the surface excess (Γ) according to de Feijter:

$$\Gamma = [(n - n_0)/(dn/dc)]d \quad (2)$$

where n_0 is the refractive indexes of the bulk solvent, and dn/dc is the refractive index increment of the adsorbing specie, for which a value of 0.148 [46] was used.

The accuracy in the thickness determination is rather high (30–35%) for small adsorbed amount (Γ < 1.0 mg/m^2), decreasing rapidly to values around 2–7% for Γ > 1.0 mg/m^2. The error in adsorbed amount is much smaller: 15% for Γ < 1.0 mg/m^2 and 0.5–2% for Γ > 1.0 mg/m^2. This is due to the fact that for low adsorbed amount, thin layers, and low optical contrasts, the refractive index of the layer and the layer thickness are coupled, due to limits of the resolution of the instrument, and it is therefore only possible to determine the adsorbed amount [47].

2.6. Laurdan generalized polarization

To gain information on lipid phase (gel, liquid-disordered and coexisting phases) as well as on transition temperature between gel and liquid-disordered phases, we used Laurdan, a polarity sensitive probe, located at the glycerol backbone of the bilayer with the lauric acid tail anchored in the phospholipid acyl chain region [48,49].

This probe doesn't show any preferential partitioning between gel and fluid phases and is considered to have uniform distribution between the inner and outer leaflets of a bilayer [49,50]. The intensity of Laurdan fluorescence is high in the visible range and is highly sensitive to the local environmental with limited scattering effects [51]. The emission spectral shift of Laurdan fluorescence mostly results from phase changes within the membrane, making it useful for discriminating between membrane phases.

Upon excitation, the dipole moment of Laurdan increases noticeably and water molecules in the vicinity of the probe reorient around this new dipole. When the membrane is in a fluid phase, the reorientation rate is faster than the emission process and, consequently, a red-shift is observed in the emission spectrum of Laurdan. When the bilayer packing increases, a part of the water molecules is excluded from the bilayer and the dipolar relaxation of the remaining water molecules is slower, leading to a fluorescent spectrum which is significantly less shifted to the red.

The steady state fluorescence parameter known as the excitation generalized polarization quantitatively relates these spectral changes by taking into account the relative fluorescence intensities of the blue and red edge regions of the emission spectra [48,49]. Excitation Generalized Polarization (GP_{ex}) was calculated using Eq. (3):

$$GP_{ex} = (I_{440} - I_{490})/(I_{440} + I_{490}) \quad (3)$$

were I_{440} and I_{490} are the fluorescence intensities at emission wavelengths of 440 nm (gel phase) and 490 nm (liquid-disordered phase), respectively.

The presence of coexisting phases is reflected by the increase of GP_{ex} upon increasing excitation wavelengths from 340 to 410. The opposite is observed when phospholipids are in the fluid-phase. When the phospholipids are in the gel phase, the GP_{ex} values don't show any change with increasing excitation wavelengths. Experiments were performed at increasing temperatures (from 5 °C to 65 °C). Monitoring GP_{ex} values as a function of temperature, also allowed to determine T_m. An adjustment to a Hill function (4) was performed:

$$GP_{ex} = GP_{ex}{}^2 + \left(GP_{ex}{}^1 - GP_{ex}{}^2\right)/\left(1 + \exp^{m\cdot(T_m - T)}\right) \quad (4)$$

where $GP_{ex}{}^1$ and $GP_{ex}{}^2$ are the maximum and minimum values of GP_{ex}, T_m, the melting temperature of the composition studied and m, the Hill coefficient. λ_{exc} was 340 nm and λ_{em} were 440 nm and 490 nm. The slope at mid-point (T_m) was calculated by the first derivative of GP_{ex} function at temperature T_m (Eq. (5)) (see [52]):

$$(dGP_{exc}/dT)_{T_m} = \left[\left(GP_{ex}{}^1 - GP_{ex}{}^2\right)\cdot m\cdot \ln 10\right]/4. \quad (5)$$

Fluorescence determinations were carried out using a thermostated Perkin-Elmer LS55 luminescence spectrometer. The lipid concentration of LUV was adjusted to 50 μM with Tris 10 mM and NaCl 150 mM at pH 8.5. Laurdan was added from a 5×10^{-3} M stock solution of DMF to give a lipid:probe ratio of 300. Surfactin was added to LUV to a final concentration of 3, 15, 25 and 100 μM and incubated under continuous agitation at 37 °C out of light for 60 min.

2.7. Atomic force microscopy

Visualization of the nanoscale effect of surfactin on membrane surface was performed using supported bilayers [41] monitored with commercial AFM (NanoScope IV MultiMode AFM, Veeco Metrology LLC, Santa Barbara, CA) equipped with a 12 μm×12 μm scanner (E-scanner). AFM images were obtained in contact mode at room temperature (23–25 °C) in Tris buffer (10 mM Tris and 150 mM NaCl at pH 8.5). All images were recorded using oxide-sharpened microfabricated Si_3N_4 cantilevers (Microlevers, Veeco Metrology LLC, Santa Barbara, CA) with spring constant of 0.01 N/m (manufacturer specified), with a minimal applied force (<500 pN) and at a scan rate of 5–6 Hz.

2.8. Molecular modeling

The "Big Monolayer" (BM) method proceeds in two steps: (i) Calculation of paired interactions between the molecules and (ii) Construction of a grid of 200×200 molecules, taking the molar ratios into account.

The first step is derived from the hypermatrix method described elsewhere [53,54]. The molecules of the system studied (surfactin, DPPC, DOPC) are first oriented at the interface, taking their hydrophobic and hydrophilic centers into account [55]. For each pair of molecules (surfactin/DPPC, surfactin/DOPC, surfactin/surfactin, DPPC/DPPC, DOPC/DOPC, and DOPC/DPPC), the interaction energies (sum of electrostatic, Van der Waals, and hydrophobic energies) are calculated for a large number of positions, resulting from translations and rotations of one molecule toward the other. In this study, we let the molecules undergo 36 rotations around themselves in steps of 10°. For each of these positions, horizontal and vertical translations are carried out on a distance of 10 and 5 Å with a step of 0.5 and 0.25 Å, respectively. For all those positions, an additional tilt of −10° to +10° by step of 0.5° is further applied. The total number of relative positions tested is thus more than 23,400,000 (36×36×21×21×41). For each pair of molecules, the statistical Boltzmann energy is considered. The latter is calculated taking into account a Boltzmann statistics corresponding to the sum of the interaction energy of each relative position tested multiplied by the probability of the position. This interaction energy matrix is then used in the second step.

The second step consists in the construction and minimization of the system using the interaction matrix calculated in step 1. A grid of 40,000 (200×200) molecules, initially positioned at random, is constructed and the energy of the system is calculated. The energy of one molecule is equal to the sum of the energies with its 24 closest neighbors in the grid. Random permutations are made and the energy of the new configuration is calculated. By a Monte Carlo procedure, this new configuration is kept or not, as a function of the energy difference between the two states. For a grid of 40,000 molecules, one calculation step consists in 40,000 permutations. 50,000 to 100,000 steps are carried out. For the molecules at the border of the grid, the molecules at the opposite border are considered as their closest neighbors, avoiding border limits.

The preferential interactions and phase separation between the molecules studied are visualized by representing each molecule type by a colored point and all the points are represented on the grid.

2.9. Diphenylhexatriene fluorescence polarization

The lipid dynamics and cooperative behavior of acyl lipid chains can be monitored by following the degree of polarization of diphenylhexatriene (DPH), a dye which probes the hydrophobic core of the membrane [56–58]. Anisotropy values (r) were determined as shown in Eq. (6):

$$r = (I_{VV} - G \cdot I_{VH})/(I_{VV} + 2 \cdot G \cdot I_{VH}) \quad (6)$$

where I_{VV} is the fluorescence intensity when angle between polarizers is 0°, I_{VH} is the fluorescence intensity when angle between polarizers is 90°, and G is an inherent factor to the fluorometer used.

T_m can be determined by monitoring anisotropy values as a function of temperature and adjustment to a Hill Eq. (7) as:

$$r = r_2 + (r_1 - r_2)/\left(1 + \exp^{m\cdot(T_m - T)}\right) \quad (7)$$

where r_1 and r_2 are the maximum and minimum values of anisotropy, T_m the melting temperature of the composition studied, and m the slope of the transition that gives information about the cooperativity of the process. The slope at T_m was calculated with the Eq. (6), which is the first derivative of the Hill equation at mid-point [52].

$$(dr/dT)_{T_m} = [(r_1 - r_2)\cdot m \cdot \ln 10]/4. \quad (8)$$

DPH was dissolved to a final concentration of 100 μM in tetrahydrofuran and added to the chloroform solution containing the lipids at a molar ratio of 300:1 (lipid:DPH) during the initial stage of preparing the vesicles (LUV) as described above. The total phospholipid concentration was adjusted to a final value of 50 μM with 10 mM Tris and 150 mM NaCl at pH 8.5. Surfactin (3, 15, 25 and 100 μM) was incubated for 60 min at 37 °C with LUV under darkness. Anisotropy (r) of samples was determined as a function of the temperature. All fluorescence determinations were performed using an LS 55 fluorescence spectrophotometer with λ_{exc} and λ_{em} of 381 nm and 426 nm, respectively.

2.10. Calcein release

Changes in the membrane permeability were followed as described by Weinstein [59]. Leakage of entrapped, self-quenched fluorescent probe, calcein, from liposomes can be monitored by the fluorescence increase as a consequence of the dilution of the probe. In these experiments the dried lipid films were hydrated with a solution of purified calcein (73 mM) in Tris 10 mM, buffer pH 8.5, which had an osmolarity of 404 mOsm/kg. The unencapsulated dye was removed from the LUV dispersion by the mini-column centrifugation technique [60]. The liposomes were diluted to a final lipid concentration of 5 μM in an isoosmotic Tris buffer (Tris 10 mM and NaCl 188 mM) pH 8.5 and equilibrated for 10 min at 25 °C. Thereafter, values were recorded for 30 s before addition of surfactin at increasing final concentrations of 3, 15, 25 or 100 μM. After the addition of surfactin, the fluorescence intensities were continuously recorded as a function of time (up to 500 s). The percentage of calcein released was determined as $[(F_t - F_{contr})/(F_{tot} - F_{contr})]\times 100$, where F_t is the fluorescence signal measured at a time t in the presence of surfactin, F_{contr} is the fluorescence signal measured at the same time t for control liposomes, and F_{tot} is the total fluorescence signal obtained after complete disruption of the liposomes by 0.02% Triton X-100. Values were fitted to a biexponential function

$$\%\,calcein\,released = y^1_{max}\left(1 - \exp^{(-k_1 t)}\right) + y^2_{max}\left(1 - \exp^{(-k_2 t)}\right) \quad (9)$$

where y^1_{max} and y^2_{max} are the maximum releases in percent due to the 1st and 2nd release mechanism respectively. k_1 and k_2 are the release constants in/s of the first and second release mechanism, respectively. t is the time in s. $t^1{}_{1/2}$ and $t^2{}_{1/2}$ are defined as the time periods for which R_{18} calcein release is doubled, respectively to the mechanism. They can be derived from $t_{1/2} = \ln 2/k$.

All fluorescence determinations were performed at 25 °C on a Perkin Elmer LS 30 Fluorescence Spectrophotometer (Perkin-Elmer Ltd., Beaconsfield, U.K.) using λ_{exc} of 472 nm and a λ_{em} of 516 nm.

2.11. Dynamic light scattering

The apparent average diameter of liposomes was estimated by dynamic light scattering using a Malvern Zetasizer Nano ZS® (Malvern Instruments, Ltd., Worcestershire, U.K.). The liposome concentration was set at 50 μM in buffer (Tris 10 mM and NaCl 150 mM at pH 8.5). Surfactin was added to liposomes at different concentrations (3, 15, 25, 75 or 100 μM). Just after mixing, dynamic light scattering was measured at an angle of 90° with monodisperse latex particles of 100 and 800 nm diameters as control. Data were analyzed using both unimodal and size distribution analysis modes to determine the mean diameter and the size distribution profile of LUVs in presence of surfactin, respectively.

2.12. Fluorescence dequenching of octadecylrhodamine B

The fusion of lipid vesicles was determined by measuring the dequenching of the fluorescence of octadecylrhodamine B chloride (R_{18}) [61]. The fluorescence of this lipid-soluble probe is self-quenched at high membrane concentration and any decrease of its surface density is therefore associated with a commensurate increase of the fluorescence intensity of the preparation [61]. Labeled LUV liposomes were obtained by incorporating R_{18} in the dry lipid film at a molar ratio of 5.7% with respect to the total lipids. The liposomes were diluted to a concentration of 10 μM in the buffer solution (Tris 10 mM and NaCl 150 mM at pH 8.5). These labeled liposomes were mixed with unlabelled LUV liposomes (adjusted to the same concentration) at a ratio of 1:4. Liposomes were equilibrated for 10 min at 25 °C. Fluorescence intensities were then recorded for 30 s before addition of surfactin at increasing concentrations (3, 15, 25 and 100 μM). Fluorescence was followed at room temperature during 200 s, using a λ_{exc} of 560 nm and a λ_{em} of 590 nm (Perkin-Elmer LS-30, Perkin-Elmer Ltd, Beaconsfield, UK). Results were expressed as percentage of R_{18} dequenching defined as $[(F_t - F_{contr})/(F_{tot} - F_{contr})] \times 100$, where F_t is the fluorescence signal measured at time t in the presence of surfactin, F_{contr} is the fluorescence signal measured at the same time t for control liposomes, and F_{tot} is the total fluorescence signal obtained after complete disruption of the liposomes by 0.02% Triton X-100. Values were fitted to an exponential function:

$$\%\, R_{18}\, dequenching = y_{max}\left(1 - \exp^{(-kt)}\right) \quad (10)$$

where y_{max} is the maximum dequenching achieved, k is the dequenching speed constant (in/s) and t the time in s. $t_{1/2}$ is defined as the time period for which R_{18} dequenching is doubled. It can be derived from $t_{1/2} = \ln 2 / k$.

3. Results and discussion

3.1. Critical micellar concentration of surfactin

It is well-known that the effect of surfactin on membranes is very dependent on the concentration [20,23–26]. Since surfactin is known to self-assembly into micelles, the first step of our study was to determine the critical micellar concentration (CMC) of the used sample of surfactin, by means of isothermal titration calorimetry. Fig. 1A shows the typical heat flow as a result of successive injections of 6 μL of surfactin 0.08 mM in a Tris 10 mM and NaCl 150 mM at pH 7.4 and 25 °C. The corresponding molar heat of demicellization ($\delta h_i/\delta n_{surf}$) as a function of surfactin concentration is shown on Fig. 1B. As the injections were performed, the absolute value of $\delta h_i/\delta n_{surf}$ decreased as the concentration of surfactin in the cell increased. This is consequence of the fact that since there is increasing number of surfactant molecules in the solution, the energy released upon break-up of the micelles decreases until it finally approaches zero at CMC. The CMC value, defined at the inflection point of the sigmoidal curve, was 2.95 ± 0.55 μM. At pH 8.5, CMC was determined to be 12.85 ± 0.05 μM. This value is higher than the value of 7.5 μM reported by Heerklotz and Seelig [19] for similar conditions (Tris 10 mM and NaCl 100 mM at pH 8.5 and 25 °C). The differences between the values found in our study and these previous data can most likely be related to the different composition of surfactin homologous in the sample used as it is well known that surfactin acyl chain length greatly influences its capacity to self-assemble into micelles [16,18].

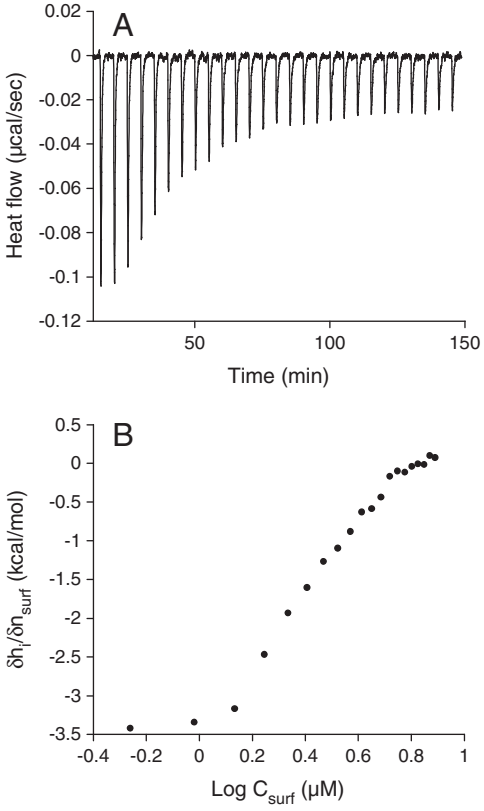

Fig. 1. CMC determination by ITC. (A) Heat flow per injection of 6 μL surfactin 0.08 mM into a 10 mM Tris and 150 mM NaCl buffer at pH 7.4 and 25 °C; and (B) Heat of injection per mole of surfactin injected versus the concentration logarithm of surfactin in the cell.

3.2. Integrity of supported phospholipid bilayers (SPBs)

In order to assess the integrity of a gel (DPPC) and a fluid (DOPC) phase lipid bilayers, the changes in thickness (d) and surface excess (Γ) of the supported DPPC or DOPC bilayer were recorded by null-ellipsometry. The effect of the sequentially increasing concentration of surfactin in the aqueous medium, at pH 7.4 was followed. Under these conditions, CMC was determined to 2.95 ± 0.55 μM at 25 °C. For each surfactin concentration, the steady state values of d and Γ obtained are reported relative to the initial values of pure SPBs (Fig. 2A and B).

The effect of surfactin on lipid bilayer was concentration dependent and was influenced by the physical state of the bilayer. Surfactin had no significant effect on both types of lipid bilayers DOPC and DPPC, at concentration lower than CMC (0.2 μM). At a concentration near the CMC (2 μM), the lipopeptide induced a low but significant decrease of both Γ and d of DOPC bilayer while it had no significant effect on DPPC bilayer. The decrease in Γ and d was more pronounced for DOPC above the CMC (10 μM). Total disintegration and removal of the DOPC bilayer was observed when the concentration of surfactin was ~6 times higher (20 μM) than CMC (Fig. 2A). At this surfactin concentration, the rate of the removal process was fast (Fig. 2C). Only 20 min were needed to totally take away the bilayer from the supporting surface. In the case of DPPC bilayer, the same concentration of surfactin (20 μM) didn't

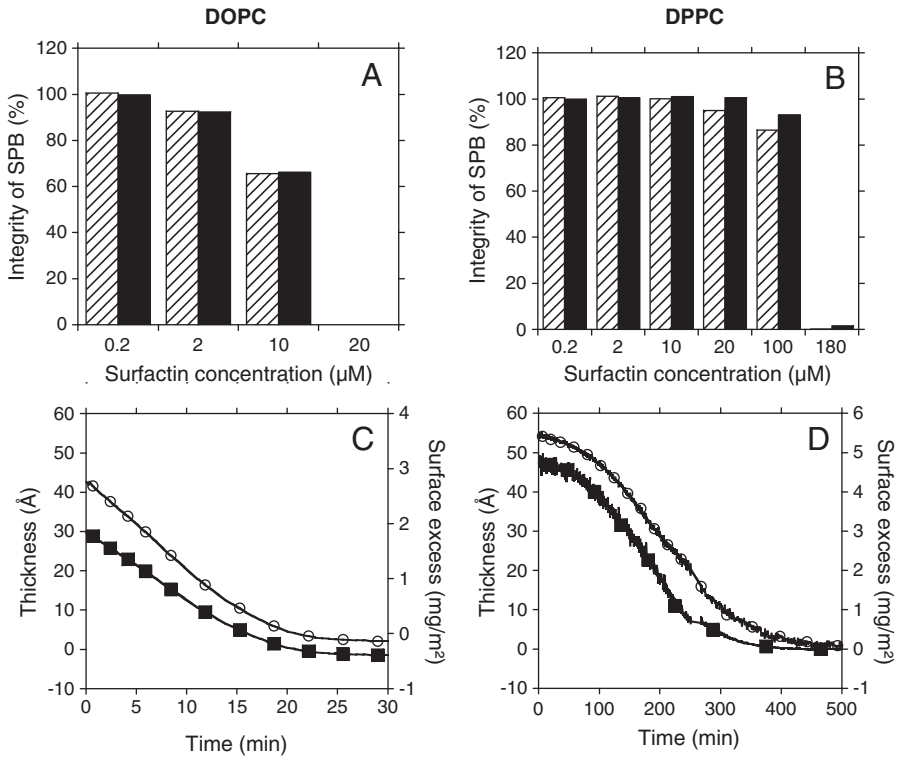

Fig. 2. Ellipsometry measurements. Top panels: Effect of surfactin concentration on supported phospholipid bilayers (SPB) integrity. Results are given in percent of bilayer thickness (striated bars) or surface excess (black bars) after addition of surfactin at different concentrations related to initial values of the pure SPB. (A) DOPC bilayer and (B) DPPC bilayer. Bottom: Time evolution of thickness (open symbols) and surface excess (closed symbols) after addition of surfactin at a critical concentration leading to a complete removal of the SPB: (C) DOPC bilayer — Final surfactin concentration in the medium = 20 μM and (D) DPPC bilayer — Final surfactin concentration in the medium = 180 μM.

influence Γ but a slight decrease of d was observed. The decrease in the bilayer thickness without removal of molecules from the supporting surface is in accordance with the model of surfactin insertion described by Heerklotz et al. [21]. In their model, surfactin molecule is rather deeply inserted into the bilayer, leading to an increasing tilt of the lipid acyl chains resulting to a decrease in the thickness. The deposited amount of DPPC bilayer was significantly decreased when 100 μM of surfactin (~33 times the CMC) was added. The complete removal of DPPC bilayer was observed when 180 μM (~60 times the CMC) of surfactin was injected (Fig. 2B). The requirement of a concentration much above the CMC to solubilize DPPC bilayer is in accordance with neutron reflectometry data obtained by Shen et al. [26]. It also took more than 300 min for the Γ and d values to reach zero (Fig. 2D). The rate of the DPPC solubilization was thus much slower than the corresponding process for DOPC.

Ellipsometry experiments clearly showed that lipid molecules in a fluid state (DOPC) are more easily solubilized by surfactin than molecules in a well-packed gel state (DPPC). The resistance of gel phases to detergent solubilization was previously described in literature for detergents (octylglucoside [62–64] or Triton X-100 [65,66]) as well as drugs like general volatile anesthetic (enflurane [67]) or lipopeptides (fengycin [68]).

3.3. Changes in bilayer packing and lipid phases induced by surfactin

The effect of surfactin concentration on lipid phases structure was investigated by monitoring the lipid phase-dependent emission spectral shift of Laurdan, which locates into the glycerol backbone region of phospholipid bilayer.

The Generalized Polarization (*GP*) makes it possible to distinguish between a mixed phase of coexisting domains, a homogeneous liquid-disordered phase and a gel phase [50]. Laurdan molecules surrounded by phospholipids in liquid-disordered and gel phases are excited in red band of the excitation spectrum. If phospholipids in gel phase are present, they mainly populate the red band of excitation, emitting with a blue spectrum and with a high *GP* value [50,69]. If no phospholipids are in the gel phase only relaxed molecules populate the red band, with a red-shifted emission spectrum and a low *GP* value. Thus, when the excitation is moved to larger wavelengths, the GP value decreases in the homogeneous liquid-disordered phase, while in bilayer composed of coexisting phases, the *GP* value increases. In gel phase, the *GP* value stays stable with the excitation wavelength [48]. Laurdan fluorescence has been monitored for liposomes composed of synthetic lipids as well as for cellular membranes [70,71] for investigating the effect of change in lipid composition (cholesterol or gangliosides e.g.) [72–74] or for characterizing effects of drugs (tamoxifen [75], propofol [76], fenitrothion [77], and phenothiazine derivatives [78] on lipid membrane organization.

The effect of surfactin on lipid phases in DOPC:DPPC (molar ratio 1:1) LUVs was investigated for surfactin concentrations lower, close and higher than CMC (3, 15, 25 and 100 μM) as function of increasing the temperature from 5 °C to 65 °C. The recorded data obtained at selected temperatures (5 °C, 25 °C, 35 °C and 55 °C) are shown (Fig. 3). Data obtained at 15 °C, 45° and 65 °C are illustrated in supplementary material. Based on these data, GP_{ex} was calculated and plotted as a function of increasing surfactin concentrations and excitation wavelengths (Fig. 3).

At 5 °C (Fig. 3A), values of GP_{ex} were around +0.4 to +0.5 with a slight increase of GP_{ex} with excitation wavelengths suggesting a high level of bilayer packing and lipid-coexisting phases. Surfactin addition at a concentration of 3 to 25 μM slightly increased the GP_{ex} values reflecting a more ordered environment at the same time as it decreased the effect of increasing excitation wavelengths on GP_{ex}, suggesting the presence of a gel phase. At 25 °C (Fig. 3B), as expected, GP_{ex} values were lower (+0.1 to +0.4) suggesting a less ordered environment.

The presence of co-existing phases was clearly observed, where DPPC gel domains were inserted in a DOPC fluid matrix. Global GP_{ex} values increased with surfactin concentrations below or close to the CMC and decreased with high surfactin concentrations, which means some ordering of the lipid phase at surfactin concentrations from 3 to 25 μM and disordering at higher concentrations (100 μM). The phase behavior tends to shift from co-existing phases towards a gel phase, as observed from the GP_{ex} values that became more and more independent of the wavelength at increasing concentrations. At 35 °C (Fig. 3C), the lipids were in fluid phase with GP_{ex} values around −0.1. A marked increase of GP_{ex} (values reached +0.3/+0.4) was observed upon increasing surfactin concentrations (from 3 to 15–25 μM), suggesting an ordering effect of surfactin with increase of packing of phospholipids. In parallel, GP_{ex} values slightly increased with the excitation wavelengths, reflecting formation of coexisting phases. The GP_{ex} was reduced at higher surfactin concentrations (100 μM) to values in the range of 0/−0.1. Simultaneously, the GP_{ex} slightly decreased with increasing excitation wavelengths, especially for wavelengths higher than 385 nm, confirming a fluidification effect of surfactin at this concentration. At higher temperatures (55 °C) (Fig. 3D), the lipids were clearly in fluid phases with GP_{ex} values around −0.2/−0.3 and increasing the surfactin concentrations didn't significantly affect lipid phase behavior.

In summary, at room temperature (25 °C), surfactin inhibited lipid-phase co-existence at concentrations close to CMC and increased GP_{ex} values, suggesting high ordering. At higher surfactin concentrations, the effect on ordering was decreased.

3.4. Nanoscale morphological changes of SPBs due to surfactin interaction

We used AFM to visualize at a nanoscale the effect of surfactin concentrations on domain formation as well as on any other morphological changes of mixed DOPC:DPPC (1:1; mol/mol) bilayers. Three defined concentrations (3 μM, 15 μM and 1 mM), i.e. below, near and far above the CMC, were selected. As shown in Fig. 4 (at time t = 0 min), the topographic image obtained for a native DOPC:DPPC (1:1 mol/mol) bilayer revealed the coexistence of two phases, the lighter and darker levels corresponding to DPPC- and DOPC-enriched phases respectively [79,80]. The step height measured between the two phases was 1.1 ± 0.1 nm and resulted from a difference in the thickness and mechanical properties of the DOPC and DPPC films [81].

Incubation of DOPC:DPPC (1:1 mol/mol) bilayers with surfactin at a concentration lower than the CMC (3 μM) caused a time-dependent erosion of the DPPC domains (Fig. 4A). It appears that the erosion phenomenon proceeds essentially at the boundary between the gel and fluid phases, thereby resulting in the disruption of the tight molecular packing of DPPC. This behavior is reminiscent of that observed with the drug azithromycin [79] and with the non-ionic detergent Triton X-100 at low concentration (half the CMC) [65]. According to Francius et al. [24], surfactin C14 at the same concentration has no effect on DOPC: DPPC bilayers. It indicates that the mixture of surfactins has a higher penetration activity than the pure surfactin C14. The high proportion of surfactin C15 that has been shown to be the most active on erythrocyte membranes [18] is likely to increase the effect of the surfactin mixture. The higher hydrophobicity but also the *iso* structure of the C15 β-hydroxy fatty acid chain can explain the higher activity of this homologue.

Notably, a very different behavior was noted near the CMC (15 μM; Fig. 4B). Twenty minutes after injection, the DPPC domains appeared to be considerably higher. The new DPPC domain height was 5.4 ± 0.2 nm, which corresponds to the thickness of a DPPC bilayer and thus indicates complete removal of the DOPC-fluid phase. At longer incubation times, a few holes appeared inside the remaining DPPC patches (see arrow in

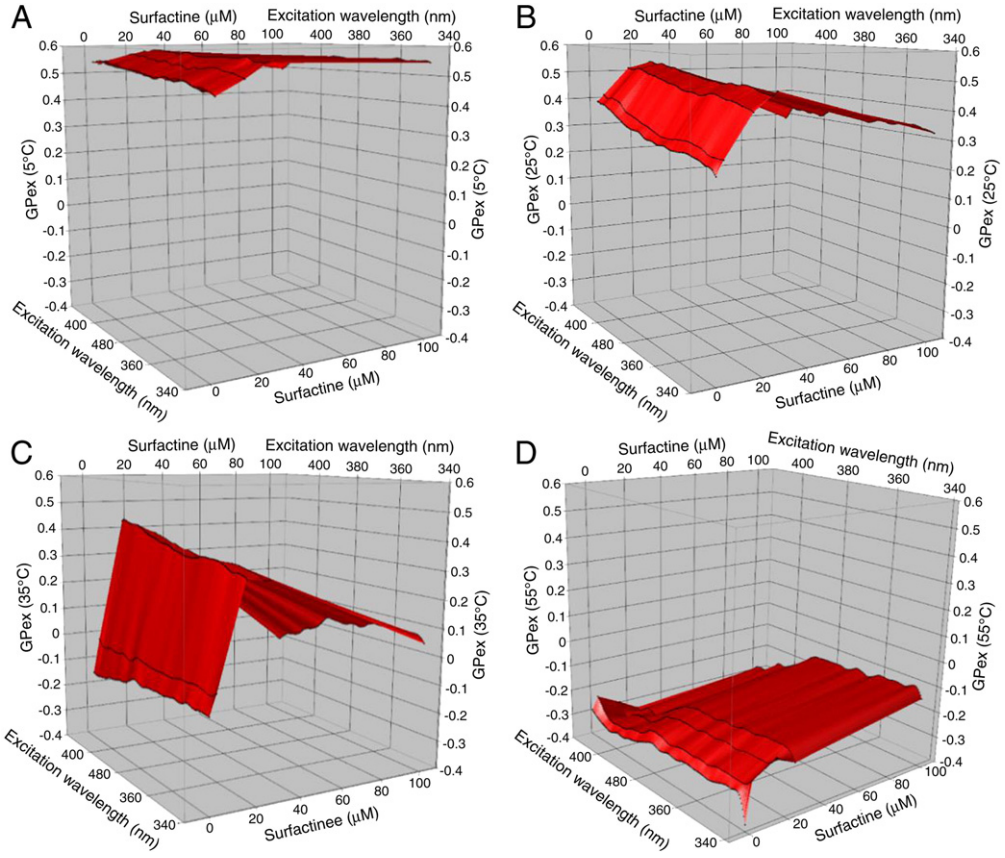

Fig. 3. Excitation generalized polarization (GP_{ex}) of Laurdan in DOPC:DPPC (1:1) in function of excitation wavelengths (from 340 nm to 410 nm) in absence and presence of increasing concentrations of surfactin (3, 15, 25, and 100 μM) at 5 °C (A), 25 °C (B), 35 °C (C), and 55 °C (D) in 10 mM Tris and 150 mM NaCl buffer at pH 8.5.

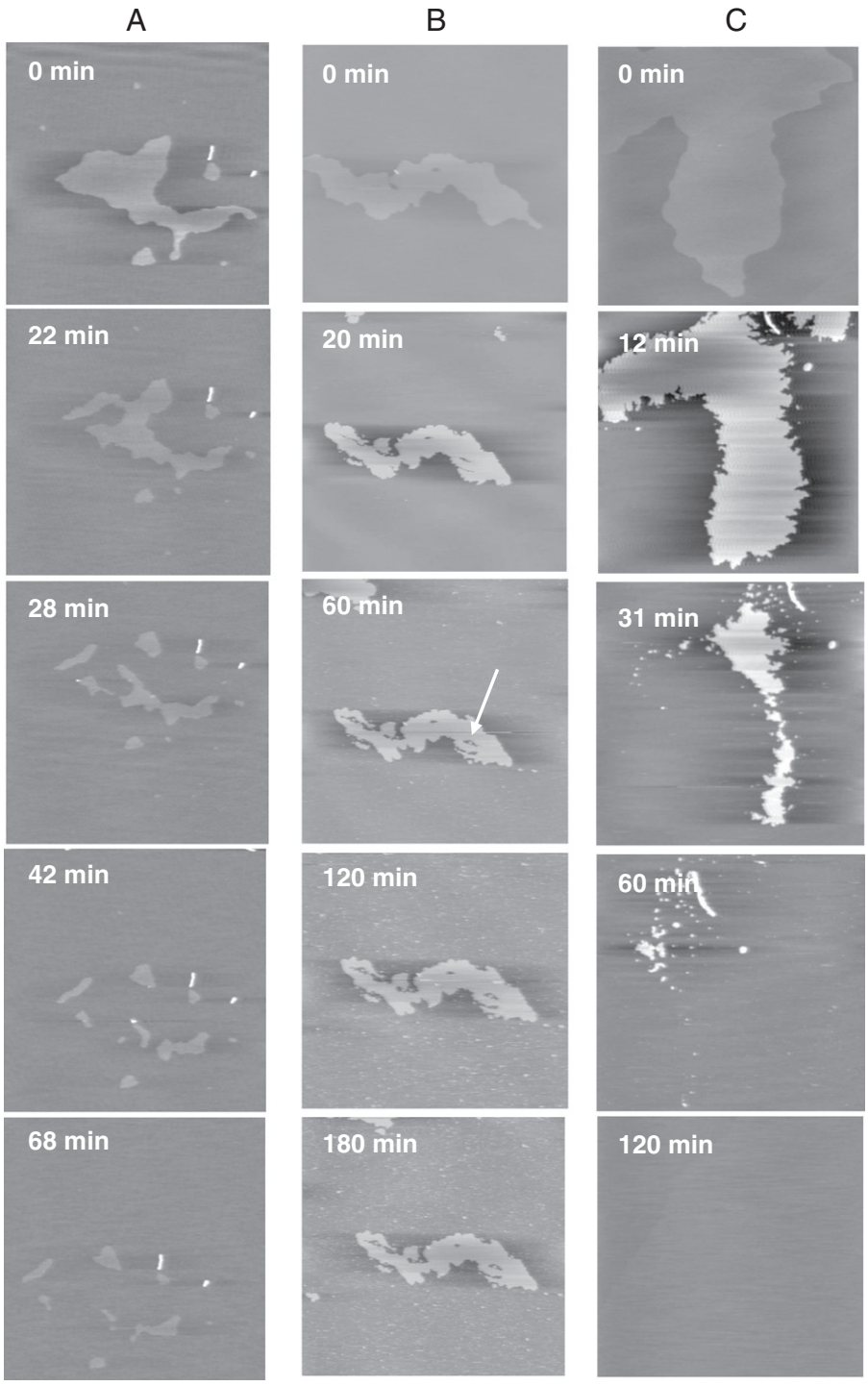

Fig. 4. AFM topographic images of a DOPC:DPPC (1:1) bilayer recorded in 10 mM Tris and 150 mM NaCl buffer at pH 8.5 (0 min) and at increasing incubation times (A) below the CMC (3 μM) (image size: 10 μm × 10 μm and z-range: 5 nm), (B) near the CMC (15 μM) (image size: at 0 min: 15 μm × 15 μm, after 0 min: 20 μm × 20 μm and z-range: 10 nm) and above the CMC (1 mM) (image size: 10 μm × 10 μm and z-range: 10 nm).

Fig. 4B), while the general shape of the domains remained essentially unaltered. Moreover, numerous white particles are observed. It is likely to be a redeposition of mixed DOPC:surfactin micelles on the mica surface [24]. These results are also very similar to those observed with Triton X-100 at a concentration 2 times greater than the CMC [65], thus indicating that surfactin, near the CMC, is able to solubilize the DOPC-fluid phase in a detergent-like manner. Finally, our results fitted well with the quantitative model reported by Keller et al. [64] which reported that order-preferring lipids like DPPC are "resistant" regardless of the presence of a second, fluid-phase lipid, like DOPC, for the action of a membrane solubilizer.

At much larger concentrations (1 mM), the DOPC-fluid phase seems to be completely removed and also the remaining DPPC domains were progressively eroded (see images recorded at 12 and 31 min; Fig. 4C) and disappeared after 60 min. No redeposition of mixed micelles or continuous bilayer was observed as was the case for octyl glucoside surfactant [82]. The dispersion of mixed DOPC:DPPC:surfactin micelles containing a high concentration of surfactin would be a stable colloidal

system in our conditions. Hence, compared with the previous situation, it appears that the detergent effect of surfactin is stronger when the concentration is well above the CMC since both DOPC and DPPC were solubilized.

AFM studies clearly revealed three major steps involved in the effect of surfactin on mixed lipid bilayers (i) erosion of DPPC domains, (ii) DOPC solubilization with removal of fluid phase and redeposition of DOPC:surfactin micelles, and (iii), erosion and disappearance of DPPC domains and dispersion of DOPC:DPPC:surfactin micelles.

3.5. Lateral distribution of surfactin within a modeled DOPC:DPPC monolayer

The effect of surfactin on the domain coexistence is confirmed by modeling the lateral distribution of surfactin within a DOPC:DPPC (1:1 mol:mol) monolayer at 25 °C. In absence of surfactin, the coexistence of segregated rounded-shape domains is observed in accordance with AFM results (Fig. 5A). For the two proportions studied (lipid:surfactin 2:0.1 and 2:0.3), surfactin molecules are localized at the boundaries between DOPC and DPPC domains (Fig. 5B and C). At higher surfactin molar ratios (Fig. 5C), an obvious changes in the shape of DOPC domains is observed suggesting that surfactin affects more strongly the fluid phase, in accordance with AFM data that, as discussed above, clearly showed a preferential solubilization of fluid lipid phase at higher surfactin concentration.

3.6. Changes in thermotropic behavior of DOPC:DPPC vesicles induced by surfactin

We determined the thermotropic effect of surfactin on both the interfacial and the hydrophobic core regions of the membrane of liposomes (DOPC:DPPC; 1:1; mol:mol) in order to further understand the nature of effect of surfactin on lipid phases observed by Laurdan fluorescence spectroscopy and visualized by AFM. For this purpose we measured the changes in GP_{ex} of the Laurdan and the fluorescence anisotropy of DPH upon temperature increase.

As previously reported for synthetic lipids (e.g. DOPC:DPPC), we clearly showed the appearance of gel and liquid phases with a defined T_m. The characteristic shape of the plot of GP_{ex} as well as fluorescence anisotropy (r) versus temperature is sigmoidal (Fig. 6), with (i) a plateau of high GP_{ex} or anisotropy values at temperatures below T_m, (ii) another plateau of low GP_{ex} or anisotropy values at temperature above T_m, and (iii) a sharp transition of GP_{ex} or anisotropy values in a short range of temperatures for which the inflexion point corresponds to T_m. The temperature dependence of Laurdan GP_{ex} as well as of DPH anisotropy provides additional information both on the apparent transition temperature and on the extent of cooperativity [83].

The GP_{ex} versus temperature is clearly dependent on the concentration of surfactin (Fig. 6A; Table 1). At 3 μM, surfactin induced a significant increase of T_m from 28.8 °C to 34.4 °C. The shift is even larger when adding a higher concentration of surfactin (15 μM) with a T_m of 39.0 °C. Above the CMC (25 μM), no further increase of T_m (38.7 °C) was recorded. At higher concentration (100 μM), T_m (29.2 °C) was similar to that of the control sample without surfactin. The highest cooperativity of the thermal transition, as determined from the slope of the steepest part of the curves in Fig. 6 (Table 1), was observed for surfactin concentrations close to CMC (15 μM). At this concentration, surfactin seems to induce a rigidifying effect both below and above T_m. For the highest concentration of surfactin (100 μM), a marked change of the trend of the curve was observed, especially at temperature above T_m, with a huge increase of GP_{ex}, reflecting an ordering effect of the interfacial region.

The DPH-steady state fluorescence anisotropy also reflected a significant increase of the T_m values from 26.6 °C to 30.2 °C (Fig. 6B; Table 1) after addition of 3 μM of surfactin. Again, the maximal increase in T_m was observed at surfactin concentration close to CMC with a T_m of 37.3 °C at 15 μM of surfactin. At 25 μM of surfactin, T_m slightly decreased to reach 34.5 °C. At the highest surfactin concentration (100 μM), the T_m value was similar (26.4 °C) to that of the surfactin free samples. For concentrations between 3 and 25 μM, both below and above T_m, a rigidifying effect was monitored.

At temperatures between 20 and 40 °C and at concentrations lower, equal or slightly higher than CMC, surfactin induced an almost similar effect on the hydrocarbon chain region (reflected by the DPH-steady state fluorescence anisotropy) as on the membrane polar surface region (as judged from the GP_{ex} data). Under these conditions and when the lipid composition is such that it mimics lipid domains found in biological membranes, surfactin was able to shift the phospholipid phase transition to higher temperature. When DOPC is solubilized from the lipid bilayer at surfactin concentrations around the CMC, one would expect that the cooperativity and transition temperature would increase as the bilayer system formed would be mostly composed of DPPC. This is exactly what we observed and what Juhastz et al. [84] reported when they decreased DOPC:DPPC ratio. In fact the transition temperature of DPPC is 41 °C which corresponds almost to value (39.0 °C) we obtained in presence of 15 μM of surfactin. Promotion of the ordered domains was also reported [85] when Triton X-100 was added to DPPC:Chol:SM vesicles i.e. when cholesterol (Chol) and sphingomyelin (SM) were present to mimic lipid domains found in biological membranes (lipid rafts), suggesting the interest of the binary lipid mixture we selected. In contrast, at conditions where DOPC was solubilized, suppressing the existence of domains, surfactin tended to shift the gel-to-liquid crystalline "melting" temperature of lipids to lower temperatures, close to value obtained for control liposomes. This behavior observed for surfactin concentrations above CMC, was similar to the effect of non-ionic detergent like Triton X-100 described by Goni et al. [86] and the effect of surfactin, on DPPC alone reported by Grau et al. [30].

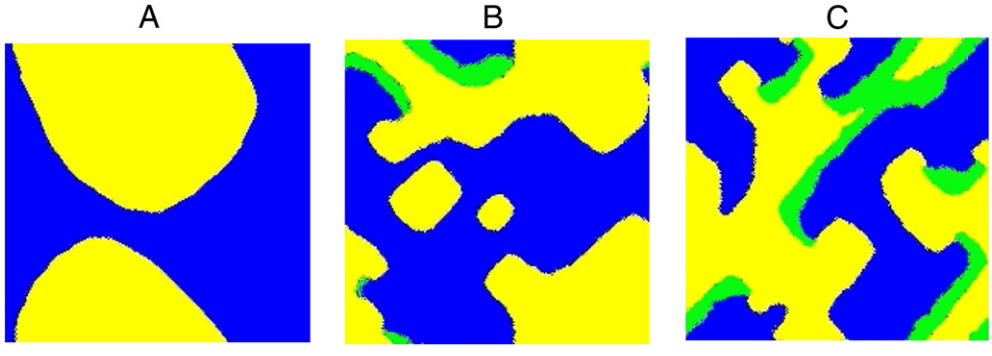

Fig. 5. Monolayer grid of 200×200 lipids calculated by the BM procedure (see Materials and methods). Each pixel represents a molecule. Blue: DPPC molecule; yellow: DOPC molecule; green: surfactin molecule. (A) DOPC:DPPC at 1:1 molar ratio, (B) DOPC:DPPC:surfactin at 1:1:0.1 molar ratio, and (C) DOPC:DPPC/surfactin at 1:1:0.3 molar ratio.

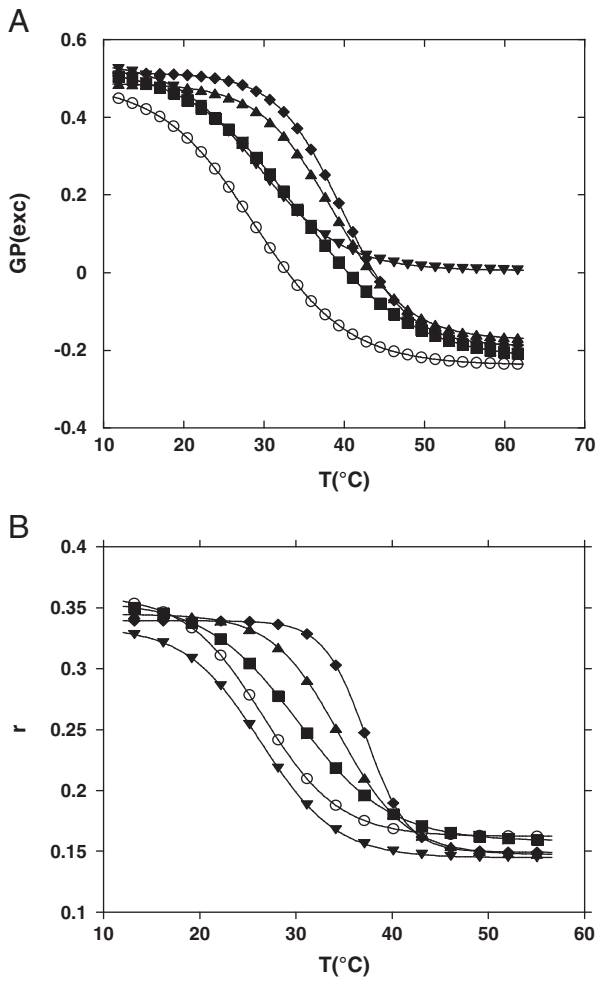

Fig. 6. Temperature-dependent Generalized Polarization (GP_{ex}) of fluorescence of Laurdan (A) and temperature-dependent fluorescence anisotropy (r) of DPH (B) in LUVs prepared from DOPC:DPPC (1:1) in 10 mM Tris and 150 mM NaCl buffer at pH 8.5 [○]. Increasing surfactin concentrations, (3 μM [■], 15 μM [◆], 25 μM [▲] and 100 μM [▼]) were added. The excitation wavelengths were 340 and 381 nm for Laurdan and DPH, respectively. The emission wavelengths were 440 and 490 nm (Laurdan) and 426 nm (DPH).

We can conclude that under conditions where lipid domains are formed, both the generalized polarization and anisotropy studies showed a marked increase of T_m induced by surfactin. The effect is very dependent on the surfactin concentration and the maximum effect was obtained for concentrations close to the CMC. For higher surfactin concentrations, when DOPC was solubilized, a clear decrease of T_m was observed.

3.7. Membrane permeability of liposomes induced by surfactin

We have previously discussed how surfactin greatly affected the organization of the lipids in supported lipid bilayers as well as in vesicles. Highly relevant from a biological activity point of view is to know if surfactin is able to induce, in our model of lipids forming phase coexistence, membrane permeabilization. For this purpose, calcein was encapsulated at a self-quenching concentration within liposomes of DOPC:DPPC (1:1 mol:mol) [59]. Surfactin was added after 30 s of recording. The best fitting of the results was obtained with a biexponential function, suggesting permeabilization took place through two processes. At the lowest concentration of surfactin investigated (3 μM), we observed a slow but steady release which reached around 75% of the maximal membrane permeabilization after 500 s (Fig. 7, Table in supplementary data). The release could involve two processes, the first one presenting a $t^1_{1/2}$ of 157.2 s and contributing to 57.5% of the absolute release, and a second one showing a $t^2_{1/2}$ of 24.9 s and contributing to 25.9% of the absolute release (Table in supplementary data). At concentrations closer to the CMC (15 and 25 μM), around 80% of calcein was released within the first 100 s (Fig. 7). The contribution of the first process to the total release of calcein became less important ~40% for 15 μM and 13.1% for 25 μM whereas the second mechanism prevailed. An increased rate of calcein release was observed upon concentration ($t^2_{1/2}$ of 12.7 and 9.8 for 15 and 25 μM, respectively) (Table in supplementary data). At concentration exceeding largely the CMC (100 μM), the release was instantaneous with the maximal release observed within the first 15 s (Fig. 7). The first process did not significantly contribute to the permeabilization, but the second one increased further in speed ($t^2_{1/2}$ of 4.8).

Below the CMC, the first release process could be governed by the insertion and accumulation of the amphiphilic molecules into the membrane. At concentrations close to or beyond the CMC, release was complete. At concentrations exceeding largely the CMC, the release was almost instantaneous. This could be due to the complete solubilisation of phospholipid vesicles and the formation of mixed micelles composed of phospholipids and surfactin, corresponding to the second release process. This behavior is close to what has been observed with Triton X-100 [87].

From a lipid self-assembly point of view, the partial membrane permeabilization induced by membrane-interacting peptides could result from two mechanisms (i) some vesicles in the population release all their aqueous contents (all-or-none mechanism), while the rest maintains the barrier intact [88], or (ii) virtually all vesicles gradually released the dye (graded mechanism) and this process is followed by an annealing process that prevents further leakage [20]. The latter mechanism is in agreement with a bilayer-couple mechanism where strain inducing leakage arises from a selective increase in the area requirement of the outer (but not the inner) leaflet by surfactin. Transient membrane failures would allow some surfactin and lipid to redistribute within membrane followed by some release of calcein from the vesicle interior. The driving force for leakage would then be reduced and the membrane would anneal and restore its integrity. Further studies aiming to

Table 1
Transition temperature and minimum slope values obtained from non-linear regression of curves from Fig. 6A and B. Comparison of values has been performed by a one-way ANOVA test. Asterisks indicate a significant difference to the control.

Surfactin concentrations	Laurdan generalized polarization		DPH anisotropy	
	$T_m \pm$ SD (°C)	Min. slope (dGP_{ex}/dT_m) ± SD	$T_m \pm$ S	Min. slope (dr/dT_m) ± SD
Control	28.8 ± 0.3	−0.031 ± 0.0005	26.6 ± 0.9	−0.013 ± 0.0004
3 μM	34.4* ± 4.9	−0.032 ± 0.0033	30.2** ± 0.3	−0.010* ± 0.0002
15 μM	39.0*** ± 2.2	−0.041 ± 0.0180	37.3*** ± 0.8	−0.022*** ± 0.0011
25 μM	38.7*** ± 1.0	−0.037 ± 0.0008	34.5*** ± 1.5	−0.015 ± 0.0009
100 μM	29.2 ± 0.5	−0.026 ± 0.0013	26.4 ± 0.9	−0.012 ± 0.0007

* $p<0.05$.
** $p<0.01$.
*** $p<0.001$.

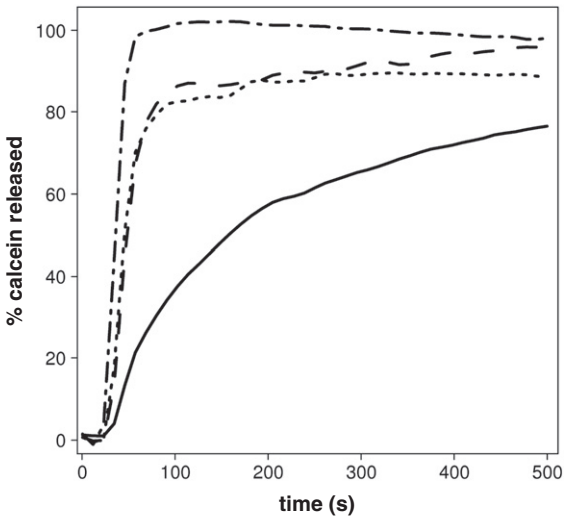

Fig. 7. Release of calcein from DOPC:DPPC (1:1) liposomes, upon addition (at t = 30s) of increasing concentrations of surfactin (3 μM [——], 15 μM [- - -], 25 μM [·····] and 100 μM [– · –]) in 10 mM Tris and 188 mM NaCl buffer at pH 8.5 and 25 °C. The recording was made for 500 s. The ordinate shows the amount of calcein released in the presence of surfactin as a percentage of the total amount released by 0.02% Triton X-100.

monitor the fluorescence lifetime of entrapped calcein as well as to visualize dye influx into individual GUVs should be done to decipher between all-or-none and graded mechanisms [88].

3.8. Fusion of LUV lipid bilayers induced by surfactin

Transient membrane discontinuities induced by surfactin insertion could be related to the propensity of membrane to fuse as reported for peptides derived from the membrane-proximal external region of HIV-1Gp41 [89]. Fusion of lipidic phase particles, e.g. vesicles, can be monitored by following the dequenching of octadecylthodamine B (R_{18}) fluorescence [61]. Aggregation of vesicles or other processes that reduce the local concentration of the fluorescent probe within the lipid bilayer could also lead to increase of fluorescence. Triton X-100 above its CMC was used as a reference for 100% dequenching since it has been shown to induce membrane fusion followed by complete solubilization of R_{18} into micelles [90].

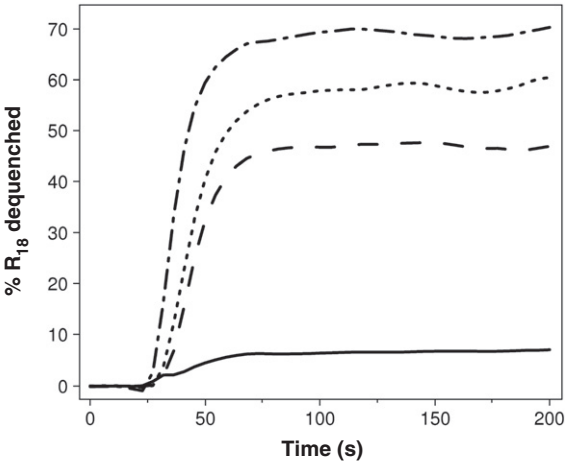

Fig. 8. Dequenching of octadecylrhodamine B (R_{18}) as a percentage of the total amount released by 0.02% Triton X-100 after addition of surfactin (t = 30s). Liposomes of DOPC:DPPC (1:1) were incubated for 200 s at 25 °C in the presence of increasing concentrations in surfactin (3 μM [——], 15 μM [- - -], 25 μM [·····] and 100 μM [– · –]) in 10 mM Tris and 150 mM NaCl buffer at pH 8.5 and 25 °C.

The values of R_{18} dequenching we observed upon addition of surfactin to DOPC:DPPC (1:1 mol:mol) vesicles are best fitted to a mono-exponential function upon time, which suggests that one primary mechanism leads to R_{18} dequenching. For surfactin concentrations below the CMC, we observed only a very small dequenching of R_{18} (max 6.8%) (Table in supplementary data) suggesting no major effect on the aggregation state of lipid dispersion (Fig. 8). Dequenching became important at CMC and for instance, at 15 μM of surfactin, it reached 47.6% that induced by Triton X-100. At 25 μM of surfactin, dequenching increased by another 12% compared to 15 μM. Further increase of surfactin concentration (100 μM) induced a faster but still partial dequenching (68.8%) [61].

However, it should be noted that many factors could influence the recorded dequenching. In particular, the dequenching properties of octadecylrhodamine can be affected by changes in lipid composition due to preferential effect of surfactin on DOPC.

3.9. Size of liposomes

To provide further insight on the relation between dequenching and vesicle aggregation/fusion, we followed the apparent size and homogeneity of the liposomes preparation incubated with surfactin, by means of dynamic light scattering, to monitor the morphological changes of DOPC:DPPC (1:1 mol:mol) vesicles induced by surfactin (Fig. 9).

Addition of 3, 15, 25 or 50 μM surfactin didn't change the DOPC:DPPC vesicle size significantly (~100 nm). At higher concentrations (75 and 100 μM) of surfactin, two main populations were observed, one with a very small mean diameter (around 10 nm) and the other with an average diameter ranging from 200 to 300 nm, suggesting the existence of fused liposomes [91].

The very small structures observed at 75 and 100 μM probably reflect mixed micelles of lipids and surfactin [19,23,25]. Indeed, surfactin should provide a solubilization of the liposome to mixed-micelles at concentrations above the CMC (25 μM) [92,93]. Once surfactin concentration within the bilayer reached a critical surfactin:lipid ratio (depending also of the lipid density and composition), surfactin molecules with their relatively large polar head compared to their small apolar chain section is expected to distort the bilayer structure. In this respect, surfactin should act as a surfactant able to solubilize phospholipid molecules.

At 25 μM, a population of small size should have been observed. However, it must be kept in mind that one limitation of dynamic light scattering technique is that results can be dominated by a small fraction of a larger species that gives a higher scattering intensity. The presence of fused vesicles or lipid aggregates can prevent the observation of individual micelles. Furthermore, since the diameters of the particles are calculated from the determined diffusion constants using Stoke–Einstein equation, which assumes spherical aggregates, the appearance of non-spherical structures would affect the calculated values of the particle diameter. Although the time-dependence of liposome solubilization by surfactin has been reported by Liu et al. [25], we found that the particle size and distribution stayed the same throughout 150 min under the conditions we used and for surfactin concentrations below 50 μM (data not shown).

At subsolubilizing concentration and based on the results from studies of surfactant induced phospholipid vesicle fusion [94], surfactin should be able to induce vesicle growth well above CMC (75 and 100 μM). Such a process has been suggested to involve surfactant-induced vesicle opening into disks stabilized on the edges by surfactants and followed by fusion of these disks if electrostatic repulsions are reduced [95]. Such a mechanism could explain the results of our dynamic light scattering data. It should also be noted that assembly of mixed lipid-surfactin micelles into a network has been reported by Boettcher et al. [96], and this also could explain the presence of larger size aggregates.

In conclusion, the results from the dynamic light scattering measurements of the mean apparent diameter of liposomes incubated with surfactin at concentrations above CMC revealed the appearance

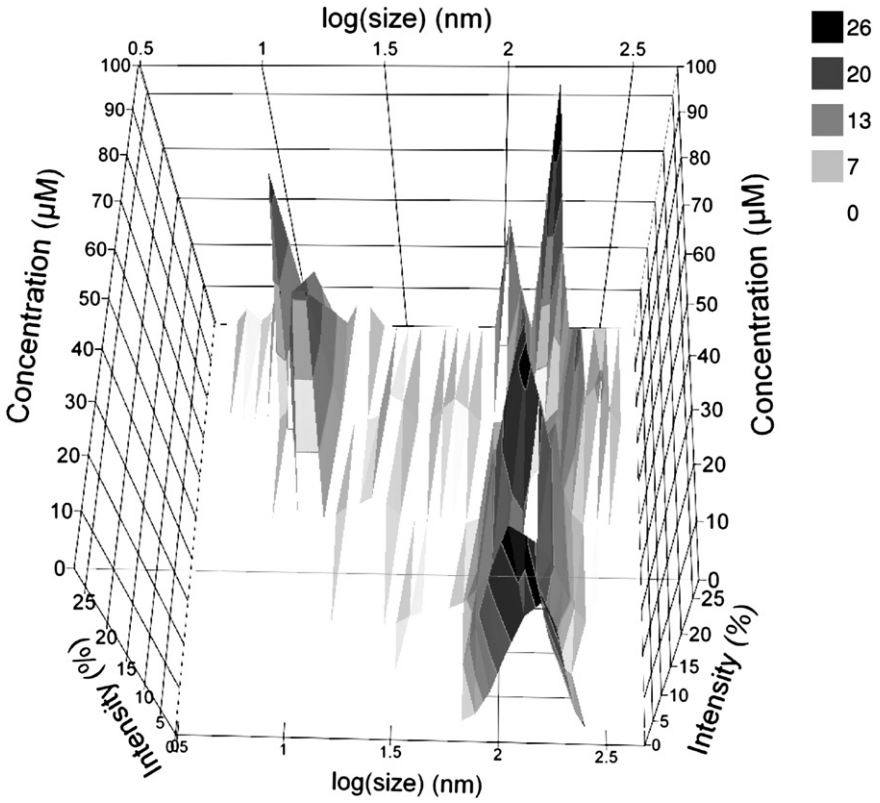

Fig. 9. Size distribution of intensity (%) upon increasing surfactin concentrations (μM) to DOPC:DPPC (1:1) vesicles in 10 mM Tris and 150 mM NaCl buffer at pH 8.5 and 25 °C. Five different levels of gray represent different limits of intensity in percent. 0% [□], 7% [▫], 13% [▪], 20% [▪] and 26%[■].

of very small structures, which are probably micelles, as well as larger structures, which could be aggregated micelles, fused liposomes or disks.

4. General discussion and conclusion

The molecular mechanism of membrane permeabilization by surfactin still remained an open question. Several viewpoints have been discussed in literature and various methods have been used to investigate this process. Most of the membrane models applied in the previous studies were composed by a single lipid and hence far from real biological membranes containing domains of different lipid phases.

In the present study, DOPC:DPPC bilayers displaying coexistence of fluid and gel domains were exploited to better understand the effect of surfactin on structural changes of biological membranes. For this purpose the effect of surfactin on lipid phases and lipid fluidity in relation to membrane integrity at the nano- and macroscopic scale was analyzed. We explored both the organization and the dynamics of DOPC:DPPC vesicles in presence of surfactin taking advantages of an array of complementary methods including Laurdan and DPH fluorescence, AFM and ellipsometry, release of calcein entrapped at self-quenching concentrations within liposomes, and dequenching of octadecylrhodamine B fluorescence.

All our observations showed that the consequences of the surfactin interaction with the membrane were highly dependent on the surfactin concentration, which confirmed previous results obtained by Francius et al. [24] and Liu et al. [25] and suggesting a detergent-like process.

A model consisting of three steps of structural and morphological changes occurring during the solubilization process and depending on the surfactin concentration can be proposed (Fig. 10) on the basis of our own and previously published findings.

First, at concentration below CMC (3 μM; Fig. 10A), binding of surfactin to the boundary between gel and fluid domains is likely to occur as suggested by AFM imaging of supported lipid bilayer domains. Data obtained by molecular modeling for two surfactin:lipid molar ratios are in accordance with this hypothesis.

The surfactin insertion at this stage makes the bilayer slightly more rigid, an effect similar to that of cholesterol [36], i.e. an increase of van der Waals interactions promotes the membrane ordering of the fluid phase. The insertion of surfactin at the boundary between DPPC and DOPC could also explain the erosion process as revealed by AFM. Liposome size was not affected by this low concentration of surfactin whereas around 85% of calcein was released. The latter observation could result from the asymmetric location of surfactin in the outer leaflet of the lipid bilayer, as the flip-flop of surfactin from the outer to the inner lipid leaflet has been reported to be limited [21,26], due to the molecular shape of surfactin. This could induce some transient perturbations leading to limited calcein release without global structural changes of the bilayer. This would correspond to the first release mechanism characterized by $t^1_{½}$ and $y^1_{max.}$

As the concentration of surfactin is increased close to CMC (15 μM at 25° C; Fig. 10B), an immediate solubilization of the fluid phase occurs. Most of DOPC molecules are solubilized and removed by surfactin and will presumably form mixed micelles. DPPC rigid domains are maintained at this surfactin concentration. This may result from unfavorable interactions between detergent and order-preferring lipid in the gel domains.

By this arrangement, surfactin induces a high ordering effect with enhancement of one gel phase, as reflected by Laurdan studies at 25 °C, probably reflecting the remaining DPPC domains. Regarding the effect on membrane permeability and as explained before, the increase in surface tension between the outer and inner leaflet as well as the curvature strain [20], due to asymmetric distribution of surfactin between inner and outer leaflet and the subsequent reorganization of lipids, were probably responsible for the membrane permeability induced by the lipopeptide

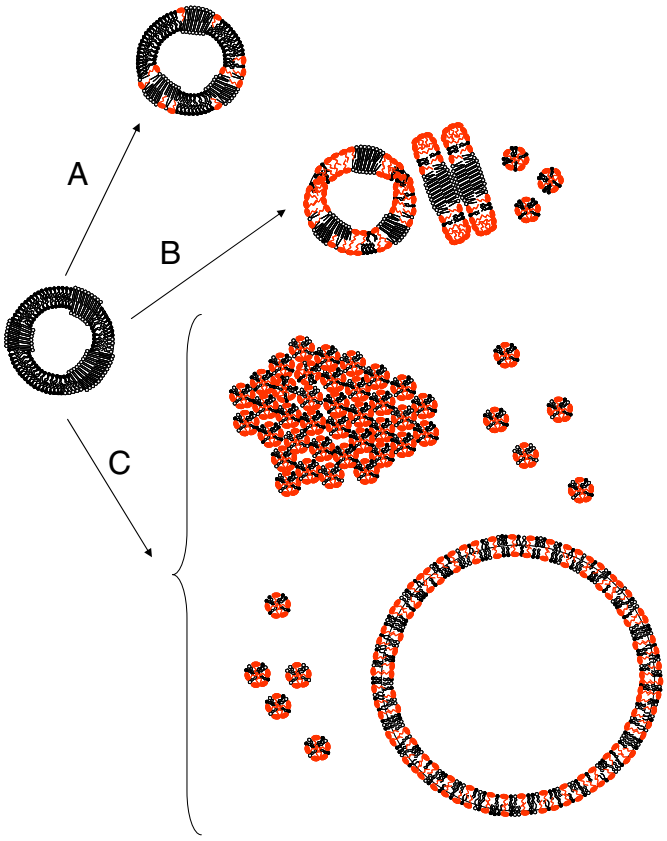

Fig. 10. Schematic model of destructuring effect of surfactin on bilayer composed by fluid and rigid domains. Surfactin concentration (A) below the CMC, (B) near the CMC, (C) well above CMC. Surfactin in red, DOPC in black and DPPC in white.

[19]. The rapid lipid fusion and the absence of effect on the liposome size could be explained by changing the lipid vesicles morphology into disks or reshaped vesicles containing surfactin and phospholipid (Fig. 10B). This could further lead to a release of calcein and might be considered as the second process contributing to calcein release and characterized by $t^2_{½}$ and $y^2_{max.}$ The existence of bilayered disk-like structures is consistent with cryo-TEM observations of Kell et al. [23] and Boettcher et al. [96].

For high surfactin concentrations (≫CMC; Fig. 10C), all the results clearly demonstrated a solubilization effect of surfactin on fluid as well as on rigid bilayers. This effect is accompanied by a marked impact on liposome size and membrane permeability. A total destabilization of the lipid bilayer occurs with a direct formation of mixed DOPC-and/or DPPC-surfactin micelles. Large particles are also formed. They can be (i) mixed micelles organized in a large network assembly (Fig. 10C top picture), in accordance with cryo-TEM images shown by Boettcher et al. [96] and/or (ii) remodeled fluid supramolecular entities with diverse morphologies (spherical (Fig. 10C bottom picture) or aspherical vesicles, open vesicles, long cylindrical micelles…) such as described by Elsayed and Cevc [97]. The second hypothesis suggests that surfactin at high concentration promotes highly curved lipid layers favoring the formation of fusion intermediates such as those suggested by Zemel et al. [98] for amphipathic peptide.

The influence of the lipid bilayer state on the solubilization by detergents is physiologically significant because tightly packed liquid ordered macro- and microdomains exist in biological membranes. These domains, believed to be rich in lipids with high phase transition temperatures, tend to be tightly packed and form liquid-ordered phase. Ellipsometry results, obtained on separated DPPC and DOPC bilayers, suggest that surfactin interacts with both bilayers in a different way. The condensed nature of the DPPC bilayer will lead to much slower diffusion rate of surfactin in the plane of the bilayer interface. DOPC bilayer on the other hand should have a lower lateral pressure than DPPC and it is also like to expose more of the hydrocarbon region to the solution. Both factors make it more favorable for surfactin binding and/or for less restricted diffusion of surfactin. This can explain the lower required surfactin concentration for the onset of fluid matrix solubilization. However, the preferential eroding action of surfactin at the boundary between DOPC and DPPC shown by AFM and molecular modeling suggests that rigid domains can play an essential role in the first step of the solubilization mechanism. Our findings are in agreement with the results from Henry et al.'s study [22], which has shown that surfactin exhibits an enhanced binding to solid ordered domains-containing vesicles and with Carillo et al.'s results [28] which suggest that DPPC acts as a promoter of surfactin-induced leakage.

Besides the effect of surfactin in the lateral plane of phospholipid bilayer, change induced by surfactin in the transversal plane of phospholipids was explored by studying the interaction of this lipopeptide with the polar head group region and hydrophobic core of phospholipids bilayer. We clearly showed the ability of surfactin, at concentrations lower or close to CMC and temperatures between 20 and 40 °C, to make the membrane regions, where Laurdan and DPH were located, more rigid with a marked increase of T_m. This is a consequence of the amphiphilic properties of surfactin and in agreement with previous studies [19]. The latter has reported that surfactin both interacts at the membrane interface and core as observed for non-ionic detergents. For concentrations much higher than CMC, we demonstrated an increase of order at the interfacial region above *Tm* whereas, within the hydrophobic core, surfactin induced a slight decrease of ordering, both below and above CMC. Our results are also in accordance with previous observations made by Fourier-transform infrared spectroscopy that reported on the incorporation of surfactin into POPC membranes [28]. The authors have shown a strong dehydration of the phospholipid C═O groups, related to a decrease in hydrogen bonding of water to the C═O groups and water penetration into the polar head group region of the membrane and hence, an ordering effect as confirmed by our Laurdan results.

In conclusion, our results give insights on the effects of a lipopeptide like surfactin, on the structure and phase behavior of model membranes composed of domain forming lipids, using Laurdan fluorescence in parallel to complementary methods such as AFM and ellipsometry. They gave rise to both a better understanding of the interaction between surfactin and lipid membrane and some insight into the molecular mechanisms leading to the biological activity of surfactin. Our findings demonstrate the crucial importance of surfactin concentration in the mechanism of membrane solubilization. However, it has to be kept in mind that solubilization is a continuous process which is also dependent on the initial aggregate size, on the transition kinetics [97] as well as on the surfactant/lipid ratio [19]. More generally, our results highlight the close relationship between the physical structure of the lipid bilayer and its association with surfactin. By affecting the lipid dynamics, surfactin could also influence the function of membrane proteins which are believed to be regulated by the phase behavior of the surrounding lipid bilayer [32].

Acknowledgements

This work was supported by the National Foundation for Scientific Research (FNRS), the Université Catholique de Louvain (Fonds Spéciaux de Recherche, Action de Recherche concertée), the Federal Office for Scientific, Technical and Cultural Affairs (Interuniversity Poles of Attraction Programme) and the Région Wallonne. R.B., Y.F.D. L.L. and M.D. are Research Director and Research Associates of the FNRS, respectively. The authors thank Marité Cardenas for theoretical and technical support for ellipsometry measurements.

Appendix A. Supplementary data

Supplementary data to this article can be found online at http://dx.doi.org/10.1016/j.bbamem.2012.11.007.

References

[1] K. Arima, A. Kakinuma, G. Tamura, Surfactin, a crystalline peptidelipid surfactant produced by *Bacillus subtilis*: isolation, characterization and its inhibition of fibrin clot formation, Biochem. Biophys. Res. Commun. 31 (1968) 488–494.

[2] A. Kakinuma, G. Tamura, K. Arima, Wetting of fibrin plate and apparent promotion of fibrinolysis by surfactin, a new bacterial peptidelipid surfactant, Experientia 24 (1968) 1120–1121.

[3] J.M. Bonmatin, M. Genest, H. Labbe, M. Ptak, Solution three-dimensional structure of surfactin: a cyclic lipopeptide studied by ^{1}H-NMR, distance geometry, and molecular dynamics, Biopolymers 34 (1994) 975–986.

[4] P. Tsan, L. Volpon, F. Besson, J.M. Lancelin, Structure and dynamics of surfactin studied by NMR in micellar media, J. Am. Chem. Soc. 129 (2007) 1968–1977.

[5] M. Kracht, H. Rokos, M. Ozel, M. Kowall, G. Pauli, J. Vater, Antiviral and hemolytic activities of surfactin isoforms and their methyl ester derivatives, J. Antibiot. Tokyo 52 (1999) 613–619.

[6] D. Vollenbroich, M. Ozel, J. Vater, R.M. Kamp, G. Pauli, Mechanism of inactivation of enveloped viruses by the biosurfactant surfactin from *Bacillus subtilis*, Biologicals 25 (1997) 289–297.

[7] D. Vollenbroich, G. Pauli, M. Ozel, J. Vater, Antimycoplasma properties and application in cell culture of surfactin, a lipopeptide antibiotic from *Bacillus subtilis*, Appl. Environ. Microbiol. 63 (1997) 44–49.

[8] A.W. Bernheimer, L.S. Avigad, Nature and properties of a cytolytic agent produced by *Bacillus subtilis*, J. Gen. Microbiol. 61 (1970) 361–369.

[9] X. Huang, Z. Wei, G. Zhao, X. Gao, S. Yang, Y. Cui, Optimization of sterilization of *Escherichia coli* in milk by surfactin and fengycin using a response surface method, Curr. Microbiol. 56 (2008) 376–381.

[10] N. Tsukagoshi, G. Tamura, K. Arima, A novel protoplast-bursting factor (surfactin) obtained from *Bacillus subtilis* IAM 1213. II. The interaction of surfactin with bacterial membranes and lipids, Biochim. Biophys. Acta 196 (1970) 211–214.

[11] A.E. Zeraik, M. Nitschke, Biosurfactants as agents to reduce adhesion of pathogenic bacteria to polystyrene surfaces: effect of temperature and hydrophobicity, Curr. Microbiol. 61 (2010) 554–559.

[12] L.K. Assie, M. Deleu, L. Arnaud, M. Paquot, P. Thonart, C. Gaspar, E. Haubruge, Insecticide activity of surfactins and iturins from a biopesticide *Bacillus subtilis* Cohn (S499 strain), Meded. Rijksuniv. Gent Fak. Landbouwkd. Toegep. Biol. Wet. 67 (2002) 647–655.

[13] Y. Imai, T. Sugino, A. Fujita, A. Kakinuma, Hypocholesterolimic effect of surfactin, a novel bacterial peptide lipid, J. Takeda Res. Lab. 30 (1971) 728–734.

[14] D.H. Kim, K.W. Yu, E.A. Bae, H.J. Park, J.W. Choi, Metabolism of kalopanaxsaponin B and H by human intestinal bacteria and antidiabetic activity of their metabolites, Biol. Pharm. Bull. 21 (1998) 360–365.

[15] M. Ongena, G. Henry, A. Adam, E. Jourdan, P. Thonart, Insights into the plant defense mechanisms induced by *Bacillus* lipopeptides, Biol. Plant–Microb. Interactions 7 (2010) 1–5.

[16] S. Dufour, M. Deleu, K. Nott, B. Wathelet, P. Thonart, M. Paquot, Hemolytic activity of new linear surfactin analogs in relation to their physico-chemical properties, Biochim. Biophys. Acta 1726 (2005) 87–95.

[17] X.H. Cao, S.S. Zhao, D.Y. Liu, Z. Wang, L.L. Niu, L.H. Hou, C.L. Wang, ROS-Ca^{2+} is associated with mitochondria permeability transition pore involved in surfactin-induced MCF-7 cells apoptosis, Chem. Biol. Interact. 190 (2011) 16–27.

[18] M. Deleu, H. Bouffioux, H. Razafindralambo, M. Paquot, C. Hbid, Ph. Thonart, Ph. Jacques, R. Brasseur, Interaction of surfactin with membranes: a computational approach, Langmuir 19 (2003) 3377–3385.

[19] H. Heerklotz, J. Seelig, Detergent-like action of the antibiotic peptide surfactin on lipid membranes, Biophys. J. 81 (2001) 1547–1554.

[20] H. Heerklotz, J. Seelig, Leakage and lysis of lipid membranes induced by the lipopeptide surfactin, Eur. Biophys. J. 36 (2007) 305–314.

[21] H. Heerklotz, A. Tsamaloukas, K. Kita-Tokarczyk, P. Strunz, T. Gutberlet, Structural, volumetric, and thermodynamic characterization of a micellar sphere-to-rod transition, J. Am. Chem. Soc. 126 (2004) 16544–16552.

[22] G. Henry, M. Deleu, E. Jourdan, P. Thonart, M. Ongena, The bacterial lipopeptide surfactin targets the lipid fraction of the plant plasma membrane to trigger immune-related defence responses, Cell. Microbiol. 13 (2011) 1824–1837.

[23] H. Kell, J.F. Holzwarth, C. Boettcher, R.K. Heenan, J. Vater, Physicochemical studies of the interaction of the lipoheptapeptide surfactin with lipid bilayers of L-alpha-dimyristoyl phosphatidylcholine, Biophys. Chem. 128 (2007) 114–124.

[24] G. Francius, S. Dufour, M. Deleu, M. Paquot, M.P. Mingeot-Leclercq, Y.F. Dufrene, Nanoscale membrane activity of surfactins: influence of geometry, charge and hydrophobicity, Biochim. Biophys. Acta 1778 (2008) 2058–2068.

[25] J. Liu, A. Zou, B. Mu, Toluidine blue: aggregation properties and distribution behavior in surfactin micelle solution, Colloids Surf. B Biointerfaces 75 (2010) 496–500.

[26] H.H. Shen, R.K. Thomas, J. Penfold, G. Fragneto, Destruction and solubilization of supported phospholipid bilayers on silica by the biosurfactant surfactin, Langmuir 26 (2010) 7334–7342.

[27] O. Bouffioux, A. Berquand, M. Eeman, M. Paquot, Y.F. Dufrene, R. Brasseur, M. Deleu, Molecular organization of surfactin-phospholipid monolayers: effect of phospholipid chain length and polar head, Biochim. Biophys. Acta 1768 (2007) 1758–1768.

[28] C. Carrillo, J.A. Teruel, F.J. Aranda, A. Ortiz, Molecular mechanism of membrane permeabilization by the peptide antibiotic surfactin, Biochim. Biophys. Acta 1611 (2003) 91–97.

[29] M. Eeman, A. Berquand, Y.F. Dufrene, M. Paquot, S. Dufour, M. Deleu, Penetration of surfactin into phospholipid monolayers: nanoscale interfacial organization, Langmuir 22 (2006) 11337–11345.

[30] A. Grau, J.C. Gomez Fernandez, F. Peypoux, A. Ortiz, A study on the interactions of surfactin with phospholipid vesicles, Biochim. Biophys. Acta 1418 (1999) 307–319.

[31] R. Maget-Dana, M. Ptak, Interactions of surfactin with membrane models, Biophys. J. 68 (1995) 1937–1943.

[32] K. Simons, W.L. Vaz, Model systems, lipid rafts, and cell membranes, Annu. Rev. Biophys. Biomol. Struct. 33 (2004) 269–295.

[33] L.A. Bagatolli, J.H. Ipsen, A.C. Simonsen, O.G. Mouritsen, An outlook on organization of lipids in membranes: searching for a realistic connection with the organization of biological membranes, Prog. Lipid Res. 49 (2010) 378–389.

[34] J. Juhasz, J.H. Davis, F.J. Sharom, Fluorescent probe partitioning in giant unilamellar vesicles of 'lipid raft' mixtures, Biochem. J. 430 (2010) 415–423.

[35] M.L. Schmidt, L. Ziani, M. Boudreau, J.H. Davis, Phase equilibria in DOPC/DPPC: conversion from gel to subgel in two component mixtures, J. Chem. Phys. 131 (Nov 2009) 175103.

[36] S. Buchoux, J. Lai-Kee-Him, M. Garnier, P. Tsan, F. Besson, A. Brisson, E.J. Dufourc, Surfactin-triggered small vesicle formation of negatively charged membranes: a novel membrane-lysis mechanism, Biophys. J. 95 (2008) 3840–3849.

[37] F. Van Bambeke, M.P. Mingeot-Leclercq, A. Schanck, R. Brasseur, P.M. Tulkens, Alterations in membrane permeability induced by aminoglycoside antibiotics: studies on liposomes and cultured cells, Eur. J. Pharmacol. 247 (1993) 155–168.

[38] H. Razafindralambo, M. Paquot, C. Hbid, P. Jacques, J. Destain, P. Thonart, Purification of antifungal lipopeptides by reversed-phase high-performance liquid chromatography, J. Chromatogr. 639 (1993) 81–85.

[39] J.P. Montenez, F. Van Bambeke, J. Piret, R. Brasseur, P.M. Tulkens, M.P. Mingeot-Leclercq, Interactions of macrolide antibiotics (Erythromycin A, roxithromycin, erythromycylamine [Dirithromycin], and azithromycin) with phospholipids: computer-aided conformational analysis and studies on acellular and cell culture models, Toxicol. Appl. Pharmacol. 156 (1999) 129–140.

[40] G.R. Bartlett, Colorimetric assay methods for free and phosphorylated glyceric acids, J. Biol. Chem. 234 (1959) 469–471.

[41] M.P. Mingeot-Leclercq, M. Deleu, R. Brasseur, Y.F. Dufrêne, Atomic force microscopy of supported lipid bilayers, Nat. Protoc. 3 (2008) 1654–1659.

[42] H.P. Vacklin, F. Tiberg, R.K. Thomas, Formation of supported phospholipid bilayers via co-adsorption with beta-D-dodecyl maltoside, Biochim. Biophys. Acta 1668 (2005) 17–24.

[43] F. Tiberg, M. Landgren, Characterization of thin nonionic surfactant films at the silica/water interface by means of ellipsometry, Langmuir 9 (1993) 927–932.

[44] M. Landgren, B. Jönsson, Determination of the optical properties of Si/SiO* surfaces by means of ellipsometry, using different ambient media, J. Phys. Chem. 97 (1993) 1656–1660.

[45] F.L. McCrackin, E. Passaglia, R.R. Stromberg, H.L. Steinberg, Measurement of the thickness and refractive index of very thin films and the optical properties of surfaces by ellipsometry, J. Res. Natl. Bur. Stand. Sect. A 67A (1963) 363–377.

[46] H.P. Vacklin, F. Tiberg, G. Fragneto, R.K. Thomas, Phospholipase A2 hydrolysis of supported phospholipid bilayers: a neutron reflectivity and ellipsometry study, Biochemistry 44 (2005) 2811–2821.

[47] P.A. Cuypers, J.W. Corsel, M.P. Janssen, J.M. Kop, W.T. Hermens, H.C. Hemker, The adsorption of prothrombin to phosphatidylserine multilayers quantitated by ellipsometry, J. Biol. Chem. 258 (1983) 2426–2431.

[48] T. Parasassi, G. De Stasio, G. Ravagnan, R.M. Rusch, E. Gratton, Quantitation of lipid phases in phospholipid vesicles by the generalized polarization of Laurdan fluorescence, Biophys. J. 60 (1991) 179–189.

[49] T. Parasassi, E. Gratton, Membrane lipid domains and dynamics as detected by Laurdan fluorescence, J. Fluoresc. 5 (1995) 59–69.

[50] L.A. Bagatolli, E. Gratton, Direct observation of lipid domains in free-standing bilayers using two-photon excitation fluorescence microscopy, J. Fluoresc. 11 (2001) 141–161.

[51] W. Yu, P.T. So, T. French, E. Gratton, Fluorescence generalized polarization of cell membranes: a two-photon scanning microscopy approach, Biophys. J. 70 (1996) 626–636.

[52] J. Giraldo, N.M. Vivas, E. Vila, A. Badia, Assessing the (a)symmetry of concentration–effect curves: empirical versus mechanistic models, Pharmacol. Ther. 95 (2002) 21–45.

[53] R. Brasseur, J.A. Killian, B. De Kruijff, J.M. Ruysschaert, Conformational analysis of gramicidin–gramicidin interactions at the air/water interface suggests that gramicidin aggregates into tube-like structures similar as found in the gramicidin-induced hexagonal HII phase, Biochim. Biophys. Acta 903 (1987) 11–17.

[54] L. Lins, A. Thomas-Soumarmon, T. Pillot, J. Vandekerchkhove, M. Rosseneu, R. Brasseur, Molecular determinants of the interaction between the C-terminal domain of Alzheimer's beta-amyloid peptide and apolipoprotein E alpha-helices, J. Neurochem. 73 (1999) 758–769.

[55] R. Brasseur, TAMMO: theoretical analysis of membrane molecular organisation, in: Molecular Description of Biological Membrane Components by Computer-aided Conformational Analysis, Brasser Edt, I and II, CRC Press, Boca Raton, Fla, 1990, pp. 203–219.

[56] R.D. Kaiser, E. London, Location of diphenylhexatriene (DPH) and its derivatives within membranes: comparison of different fluorescence quenching analyses of membrane depth, Biochemistry 37 (1998) 8180–8190.

[57] B.R. Lentz, Use of fluorescent probes to monitor molecular order and motions within liposome bilayers, Chem. Phys. Lipids 64 (1993) 99–116.

[58] M. Shinitzky, Y. Barenholz, Fluidity parameters of lipid regions determined by fluorescence polarization, Biochim. Biophys. Acta 515 (1978) 367–394.

[59] J.N. Weinstein, S. Yoshikami, P. Henkart, R. Blumenthal, W.A. Hagins, Liposome–cell interaction: transfer and intracellular release of a trapped fluorescent marker, Science 195 (1977) 489–492.
[60] P.I. Lelkes, Methodogical aspects dealing with stability measurements of liposomes in vitro using the carboxyfluorescein assay, in: Liposome Technology, Gregoriadis Edts, 3, CRC Press, 1984, pp. 225–246.
[61] D. Hoekstra, T. de Boer, K. Klappe, J. Wilschut, Fluorescence method for measuring the kinetics of fusion between biological membranes, Biochemistry 23 (1984) 5675–5681.
[62] M.L. Jackson, B.J. Litman, Rhodopsin–phospholipid reconstitution by dialysis removal of octyl glucoside, Biochemistry 21 (1982) 5601–5608.
[63] M.L. Jackson, C.F. Schmidt, D. Lichtenberg, B.J. Litman, A.D. Albert, Solubilization of phosphatidylcholine bilayers by octyl glucoside, Biochemistry 21 (1982) 4576–4582.
[64] S. Keller, A. Tsamaloukas, H. Heerklotz, A quantitative model describing the selective solubilization of membrane domains, J. Am. Chem. Soc. 127 (2005) 11469–11476.
[65] S. Morandat, K. El Kirat, Membrane resistance to Triton X-100 explored by real-time atomic force microscopy, Langmuir 22 (2006) 5786–5791.
[66] E. Schnitzer, D. Lichtenberg, M.M. Kozlov, Temperature-dependence of the solubilization of dipalmitoylphosphatidylcholine (DPPC) by the non-ionic surfactant Triton X-100, kinetic and structural aspects, Chem. Phys. Lipids 126 (2003) 55–76.
[67] N. Hauet, F. Artzner, F. Boucher, C. Grabielle-Madelmont, I. Cloutier, G. Keller, P. Lesieur, D. Durand, M. Paternostre, Interaction between artificial membranes and enflurane, a general volatile anesthetic: DPPC–enflurane interaction, Biophys. J. 84 (2003) 3123–3137.
[68] M. Deleu, M. Paquot, T. Nylander, Effect of fengycin, a lipopeptide produced by *Bacillus subtilis*, on model biomembranes, Biophys. J. 94 (2008) 2667–2679.
[69] T. Parasassi, G. Ravagnan, R.M. Rusch, E. Gratton, Modulation and dynamics of phase properties in phospholipid mixtures detected by Laurdan fluorescence, Photochem. Photobiol. 57 (1993) 403–410.
[70] G. Balogh, G. Maulucci, I. Gombos, I. Horvath, Z. Torok, M. Peter, E. Fodor, T. Pali, S. Benko, T. Parasassi, M. De Spirito, J.L. Harwood, L. Vigh, Heat stress causes spatially-distinct membrane re-modelling in K562 leukemia cells, PLoS One 6 (2011) e21182.
[71] K. Gaus, E. Gratton, E.P. Kable, A.S. Jones, I. Gelissen, L. Kritharides, W. Jessup, Visualizing lipid structure and raft domains in living cells with two-photon microscopy, Proc. Natl. Acad. Sci. U. S. A. 100 (2003) 15554–15559.
[72] L.A. Bagatolli, S.A. Sanchez, T. Hazlett, E. Gratton, Giant vesicles, Laurdan, and two-photon fluorescence microscopy: evidence of lipid lateral separation in bilayers, Methods Enzymol. 360 (2003) 481–500.
[73] C. Dietrich, L.A. Bagatolli, Z.N. Volovyk, N.L. Thompson, M. Levi, K. Jacobson, E. Gratton, Lipid rafts reconstituted in model membranes, Biophys. J. 80 (2001) 1417–1428.
[74] K.K. Halling, B. Ramstedt, J.H. Nystrom, J.P. Slotte, T.K. Nyholm, Cholesterol interactions with fluid-phase phospholipids: effect on the lateral organization of the bilayer, Biophys. J. 95 (2008) 3861–3871.
[75] M. Engelk, P. Bojarski, R. Bloss, H. Diehl, Tamoxifen perturbs lipid bilayer order and permeability: comparison of DSC, fluorescence anisotropy, Laurdan generalized polarization and carboxyfluorescein leakage studies, Biophys. Chem. 90 (2001) 157–173.
[76] S.V. Balasubramanian, R.B. Campbell, R.M. Straubinger, Propofol, a general anesthetic, promotes the formation of fluid phase domains in model membranes, Chem. Phys. Lipids 114 (2002) 35–44.
[77] M.R. Gonzalez-Baro, H. Garda, R. Pollero, Effect of fenitrothion on dipalmitoyl and 1-palmitoyl-2-oleoylphosphatidylcholine bilayers, Biochim. Biophys. Acta 1468 (2000) 304–310.
[78] A.B. Hendrich, K. Michalak, O. Wesolowska, Phase separation is induced by phenothiazine derivatives in phospholipid/sphingomyelin/cholesterol mixtures containing low levels of cholesterol and sphingomyelin, Biophys. Chem. 130 (2007) 32–40.
[79] A. Berquand, M.P. Mingeot-Leclercq, Y.F. Dufrene, Real-time imaging of drug–membrane interactions by atomic force microscopy, Biochim. Biophys. Acta 1664 (2004) 198–205.
[80] M.C. Giocondi, L. Pacheco, P.E. Milhiet, C. Le Grimellec, Temperature dependence of the topology of supported dimirystoyl–distearoyl phosphatidylcholine bilayers, Ultramicroscopy 86 (2001) 151–157.
[81] Y.F. Dufrene, A. van der Wal, W. Norde, P.G. Rouxhet, X-ray photoelectron spectroscopy analysis of whole cells and isolated cell walls of Gram-positive bacteria: comparison with biochemical analysis, J. Bacteriol. 179 (1997) 1023–1028.
[82] S. Morandat, K. El Kirat, Solubilization of supported lipid membranes by octyl glucoside observed by time-lapse atomic force microscopy, Colloids Surf. B Biointerfaces 55 (2007) 179–184.
[83] S. Mukherjee, A. Chattopadhyay, Monitoring the organization and dynamics of bovine hippocampal membranes utilizing Laurdan generalized polarization, Biochim. Biophys. Acta 1714 (2005) 43–55.
[84] J. Juhasz, J.H. Davis, F.J. Sharom, Fluorescent probe partitioning in GUVs of binary phospholipid mixtures: implications for interpreting phase behavior, Biochim. Biophys. Acta 1818 (2012) 19–26.
[85] H. Heerklotz, Triton promotes domain formation in lipid raft mixtures, Biophys. J. 83 (2002) 2693–2701.
[86] F.M. Goni, M.A. Urbaneja, J.L. Arrondo, A. Alonso, A.A. Durrani, D. Chapman, The interaction of phosphatidylcholine bilayers with Triton X-100, Eur. J. Biochem. 160 (1986) 659–665.
[87] G.M. Alder, W.M. Arnold, C.L. Bashford, A.F. Drake, C.A. Pasternak, U. Zimmermann, Divalent cation-sensitive pores formed by natural and synthetic melittin and by Triton X-100, Biochim. Biophys. Acta 1061 (1991) 111–120.
[88] H. Patel, C. Tscheka, K. Edwards, G. Karlsson, H. Heerklotz, All-or-none membrane permeabilization by fengycin-type lipopeptides from *Bacillus subtilis* QST713, Biochim. Biophys. Acta 1808 (2011) 2000–2008.
[89] B. Apellaniz, S. Nir, J.L. Nieva, Distinct mechanisms of lipid bilayer perturbation induced by peptides derived from the membrane-proximal external region of HIV-1 gp41, Biochemistry 48 (2009) 5320–5331.
[90] T. Buranda, Y. Wu, D. Perez, A. Chigaev, L.A. Sklar, Real-time partitioning of octadecyl rhodamine B into bead-supported lipid bilayer membranes revealing quantitative differences in saturable binding sites in DOPC and 1:1:1 DOPC/SM/cholesterol membranes, J. Phys. Chem. B 114 (2010) 1336–1349.
[91] F. Van Bambeke, P.M. Tulkens, R. Brasseur, M.P. Mingeot-Leclercq, Aminoglycoside antibiotics induce aggregation but not fusion of negatively-charged liposomes, Eur. J. Pharmacol. 289 (1995) 321–333.
[92] A. De la Maza, J.L. Parra, Vesicle–micelle structural transition of phosphatidylcholine bilayers and Triton X-100, Biochem. J. 303 (1994) 907–914.
[93] U. Kragh-Hansen, M. le Maire, J.V. Moller, The mechanism of detergent solubilization of liposomes and protein-containing membranes, Biophys. J. 75 (1998) 2932–2946.
[94] M. Silvander, K. Edwards, A method to detect leakage of DNA intercalators through liposome membranes, Anal. Biochem. 242 (1996) 40–44.
[95] K. Edwards, J. Gustafsson, M. Almgren, G. Karlsson, Solubilization of lecithin vesicles by a cationic surfactant — intermediate structures in the vesicle micelle transition observed by cryo-transmission electron microscopy, J. Colloid Interface Sci. 161 (1993) 299–309.
[96] C. Boettcher, H. Kell, J.F. Holzwarth, J. Vater, Flexible loops of thread-like micelles are formed upon interaction of L-alpha-dimyristoyl-phosphatidylcholine with the biosurfactant surfactin as revealed by cryo-electron tomography, Biophys. Chem. 149 (2010) 22–27.
[97] M.M. Elsayed, G. Cevc, The vesicle-to-micelle transformation of phospholipid-cholate mixed aggregates: a state of the art analysis including membrane curvature effects, Biochim. Biophys. Acta 1808 (2011) 140–153.
[98] A. Zemel, A. Ben Shaul, S. May, Modulation of the spontaneous curvature and bending rigidity of lipid membranes by interfacially adsorbed amphipathic peptides, J. Phys. Chem. B 112 (2008) 6988–6996.